Structure, Dynamics and Free Energy Studies on the Effect of Spot Mutations on SARS-CoV-2 Spike Protein Binding with ACE2 Receptor

Short title: Structure, Dynamics and Free Energy Studies on RBD Variants Binding with ACE2

George Rucker[1], Hong Qin[2], Liqun Zhang[3]

1. Chemical Engineering Department, Tennessee Technological University, Cookeville, TN, 38501
2. Computer Science department, University of Tennessee Chattanooga, Chattanooga, TN 37403
3. Chemical Engineering Department, University of Rhode Island, Kingston, RI, 02881

Corresponding author: Liqun Zhang

Email: zhangl@uri.edu

Abstract

The ongoing COVID-19 pandemic continues to infect people worldwide, and the virus continues to evolve in significant ways which can pose challenges to the efficiency of available vaccines and therapeutic drugs and cause future pandemic. Therefore, it is important to investigate the binding and interaction of ACE2 with different RBD variants. A comparative study using all-atom MD simulations was conducted on ACE2 binding with 8 different RBD variants, including N501Y, E484K, P479S, T478I, S477N, N439K, K417N and N501Y-E484K-K417N on RBD. Based on the RMSD, RMSF, and DSSP results, the overall the binding of RBD variants with ACE2 is stable, and the secondary structure of RBD and ACE2 are consistent after the spot mutation. Besides that, a similar buried surface area, a consistent binding interface and a similar amount of hydrogen bonds formed between RBD with ACE2 although the exact residue pairs on the binding interface were modified. The change of binding free energy from spot mutation was predicted using the free energy perturbation (FEP) method. It is found that N501Y, N439K, and K417N can strengthen the binding of RBD with ACE2, while E484K and P479S weaken the binding, and S477N and T478I have negligible effect on the binding. Spot mutations modified the dynamic correlation of residues in RBD based on the dihedral angle covariance matrix calculation. Doing dynamic network analysis, a common intrinsic network community extending from the tail of RBD to central, then to the binding interface region was found, which could communicate the dynamics in the binding interface region to the tail thus to the other sections of S protein. The result can supply unique methodology and molecular insight on studying the molecular structure and dynamics of possible future pandemics and design novel drugs.

Introduction

48 COVID-19 pandemic which is the result of infection by SARS-Coronavirus-2 (CoV-2), had
49 claimed over 6 million lives as of June 2023, and continues impacting worldwide health [1]. CoV-2
50 expresses S (Spike) protein [2,3], which is responsible for binding to the host cell receptor followed
51 by fusion of the viral and cellular membranes, respectively [4]. To engage a host cell receptor, the
52 receptor-binding domain (RBD) of the S protein undergoes hinge-like conformational movements
53 [5], thus mediates interaction with the receptor angiotensin-converting enzyme 2 (ACE2) [6,7,8,9]
54 (the RBD and ACE2 binding structure is shown in Figure 1 (a)). The binding of RBD with ACE2
55 is believed to be the critical initial event in the infection cascade. The interface residues on RBD
56 thus play key roles in the spike protein's binding with ACE2.

57 Coronaviruses are enveloped viruses that possess a positive-sense single-stranded RNA genome
58 26–32 kb in length [10], and have a remarkable mutation rate that allows them to evolve in a way
59 that perhaps by increasing their transmissibility [11,12, 13, 14] and/or their resistance to protective
60 immunity induced by previous infection or vaccines [15, 16, 17, 18, 19, 20]. Up to now, different
61 variants of concern (VOCs) have shown up, including Alpha, Beta, Gamma, Delta, and Omicron
62 [21,22,23,24,25,26,27,28] (Some mutations involved are shown in Table S1 in SI). The Alpha
63 variant was found in UK in September of 2020, while Beta variant was found in North Africa in
64 May of 2020. Gamma variant was found in Brazil[21,22,23,25]. The Omicron variant which
65 contains 11 mutants on RBD, is still the dominant cause of the resurgence of infection in many
66 countries currently [27]. Most of the mutations (around 58% of mutations) on RBD are located at
67 the receptor binding motif which is the binding interface with ACE2 [29].

68 N501Y on RBD, which appeared in Alpha, Beta, Gamma and Omicron variants, increased the
69 binding affinity of RBD with ACE2 [30, 31] and enhanced the viral resistance to neutralizing
70 antibodies [32]. S477N appeared in Omicron and E484K appeared in both Beta and Gamma

71 variants, were reported to enhance the binding affinity of S protein with ACE2 [33,34]. K417N
72 found in both Beta and Omicron variants was reported to decrease the binding affinity of RBD and
73 ACE2 [35], and was thought to cause immune escape [36]. The triple mutants of N501Y-E484K-
74 K417N appeared in Beta variant, has been shown to increase the infectivity of virus considering
75 the effect of each single mutants [35]. N439K, which was found in multiple regions in the world
76 and a quite common mutation, can enhance the binding of RBD with human ACE2 receptor while
77 evade antibody mediated immunity [37]. P479S, which also happened with high frequency at
78 most countries based on SARS-CoV-2 genome samples deposited at GISAID in early 2020 [38],
79 was predicted to make the virus less infective based on algebraic topology-based machine learning
80 modelling [29]. Besides that, based on the report of most frequently occurring mutations in RBD
81 in January 2021 (https://www.gisaid.org/hcov19-mutation-dashboard), T478I which appeared in
82 Alpha variant, however did not influence the binding of RBD and ACE2 [39]. Those mutants all
83 appeared in RBD binding interface.

84 Besides those experimental work, in order to find out the mechanism of CoV-2 variants binding
85 with ACE2 and to design effective therapeutics to deal with CoV-2 variants, molecular dynamics
86 simulation methods have been applied to study RBD binding with ACE2 [33,40,41,34,42,
87 43,44,45,46,47]. Different simulation methods were used to predict the binding free energy change
88 ($\Delta\Delta G$) [48, 49], including free energy perturbation (FEP) method [43,41], molecular mechanics
89 Poisson-Boltzmann surface area (MM-PBSA) method [42], molecular mechanics-generalized
90 Born surface area (MM/GBSA) method [45] and so on. Li et al. [49] and other researchers found
91 that FEP method can predict $\Delta\Delta G$ reasonably [41,48, 50] and better than other methods [49]. Thus
92 FEP method was applied to predict the spot mutation on RBD to the binding of RBD variants with
93 ACE2 in this work. Besides that, dynamic correlation was calculated to predict correlation matrix

94 and dynamic network in RBD and ACE2 in order to understand how the S spike mutants on RBD
95 binding interface can affect the binding of RBD with ACE2. Since spot mutations happened quite
96 often on CoV-2 RBM [29], a comparative study on multiple single mutations on RBD binding
97 with ACE2 is necessary. In total 7 RBD single mutants which happened naturally and can
98 potentially affect the binding and dynamics of RBD with ACE2 were studied including N501Y,
99 E484K, K417N, N439K, P479S, T478I, S477N, and one triple mutant N501Y-E484K-K417N.
100 Their effects on the binding of RBD with ACE2 were analyzed. Besides all-atom NAMD
101 simulations, FEP method was applied to predict ΔΔG of RBD with ACE2 because of the spot
102 mutation. The simulation predictions helped to clarify the contradicting available experimental
103 results. Calculating the dihedral angle covariance matrices and doing dynamic network analysis,
104 an intrinsic network community was predicted. Our results revealed the molecular mechanism
105 that underlies the dynamics and energy change of some RBD variants binding with ACE2. Such
106 kind of information will be valuable for the development of further vaccines and neutralizing
107 antibodies against mutant forms of the SARS-CoV-2 virus.

108

109 **Figure 1**. The binding structure of ACE2 (in blue) with RBD (in green) (a), with the mutations
110 (shown in red sticks) on RBD labeled; and the comparison of the initial and final structures of
111 ACE2 bound with RBD tri-mutant variant (b). In b), the initial structures of ACE2 and RBD are
112 shown in wheat, and the final structure of ACE2 is shown in raspberry and magenta for RBD. The
113 mutants of E484K, K417N, and N501Y are shown in blue sticks in both the initial and final
114 structures.

115

Materials and Methods

1). Based on the survey up to now, 7 naturally happened single RBD mutants were studied: E484K, N439K, P479S, T478I, N501Y, K417N, S477N, besides one triple mutants of RBD which has E484K, N501Y and K417N. The selection of those mutations is based on different SARS-CoV-2 variants shown as listed in Table S1 in SI. The mutation sites on ACE2 and RBD binding interface are shown in Figure 1(a). The crystal structure of the RBD domain of the Spike protein is available in complex with ACE2 at 2.45 Å resolution in the PDB with ID 6M0J [51], which was used as the starting structure to build the RBD mutants bound with ACE2. VMD program [52] was applied to mutate residues on RBD to generate RBD mutants. The corresponding RBD and ACE2 structures in [51] were used in reference simulations of RBD and ACE2 in free forms respectively. The bound and free forms of simulations conducted in this project are listed in Table S2.

Different simulation systems were set up using VMD program and CHARMM36m forcefield [53]. The system was solvated with enough amount of TIP3P water molecules with the minimum distance between protein and water box edge being at least 12 Å, and was neutralized with 0.15M NaCl solvent. After a brief energy minimization using the conjugate gradient and line search algorithm, 4 ps of dynamics was run at 50 K, and then the system was brought up to 310 K over an equilibration period of 1 ns using NAMD program[54], all-atom molecular dynamics simulation was performed on each system using NAMD program and CHARMM36 forcefield [55]. The temperature was 310K and a desired pressure of 1 atm using standard thermo- and barostats. The sampling run was 100 ns with a time step of 1 fs. The trajectory output frequency was 1 ps. To do comparisons on the binding of RBD mutant with ACE2, the RBD bound with ACE2 wildtype systems were also set up and simulations were performed for 100 ns for RBD mutant & ACE2.

138 The simulation systems, set up, the number of atoms and box size information are shown in Table
139 S2.
140 To analyze the trajectories, the Root Mean Square Deviation (RMSD) and Fluctuations (RMSF)
141 of the proteins were calculated using the VMD program and an in-house analysis script based on
142 the coordinates of the backbone Ca atoms after aligning the trajectories respectively, to the original
143 crystal structure of the RBD, ACE2, and to the initial complex structure of the RBD and ACE2
144 from Lan et al.[51]. The buried surface area (BSA) for the complex was calculated in two steps
145 using the VMD program and a script using the Richards and Lee method with the water probe size
146 of 1.4 Å (Lee and Richards, 1971). First, the total solvent accessible surface area of the complex
147 ($ASA_{complex}$) was calculated based on the complex's trajectory. Second, the accessible surface area
148 of each protein in the complex (ASA_{rbd}, ASA_{ACE2}) was calculated for each protein individually.
149 Then, the buried surface area (BSA) is calculated using Equation (1):
150
151 $$BSA=0.5*(ASA_{rbd} + ASA_{ACE2} - ASA_{complex}) \quad (1)$$
152
153 The number of hydrogen bonds between the RBD and ACE2 were calculated using the VMD
154 program with the heavy atom distance cutoff of 3.0 Å and the angle cutoff of 20 degrees deviation
155 from H-bond linearity. The time a particular H-bond is formed over the course of the simulation
156 is monitored and is expressed as % occupancy. In order to find out the residues on the binding
157 interface, the closest distance between every residue atom (including hydrogen) between the RBD
158 and ACE2 was calculated and averaged over the trajectory run. The average distances between
159 each residue on RBD and on ACE2 are shaded by proximity on a red to white color-scale and were
160 used to build the distance maps.

2). Dihedral Angle Correlation, network community calculation. To quantitatively describe the motional correlations of the backbone in RBD, we calculated the ϕ and ψ cross-correlation matrix for all the residues except the first or last one on the sequence. ϕ describes the rotation of the N−Cα bond and involves the CO−N−Cα−CO bonds. ψ describes the rotation of Cα and the CO bond and involves the N−Cα−CO−N bonds. Both ϕ and ψ were calculated for residues at different times using the wordom program [56,57]. Because both ϕ and ψ are angular variables, to avoid the periodicity problem, the circular correlation coefficient, which is a T-linear dependence, was calculated in this project following the method of Fisher [58,59] and Mardia and Jupp[60], and in the same way as in our previous work [61,62]. The $\phi-\varphi$ cross-correlation coefficients (matrices) were calculated of all combinations of dihedral angles. In order to simplify the data representation, the $\phi-\phi$, $\phi-\varphi$, and $\varphi-\varphi$ correlation matrices were combined and the element with the largest magnitude at residue pair position was always chosen to build the final matrix.

In the dynamic network community calculation, the network model was built by the NetworkView plug-in of VMD [63] and the program Carma [64]. In the network, the nodes could be considered as a single atom or a cluster of atoms. In this project, each Cα atom in one amino acid was treated as one node. The edge between two nodes was defined with the cutoff distance of 4.5Å for at least 75% of molecular dynamics simulated trajectory.

3). In order to find out the contribution of mutant residues on RBD to its binding with ACE2, FEP method has been applied in the same way as in [50]. The change of free energy of each mutation to the binding was predicted, including E484K, N439K, N501Y, P479S, S477N, T478I, K417N on RBD binding with ACE2.

183 In total, two kinds of systems were set up. One is the RBD in wildtype form in solvent (unbound
184 state). The other is the RBD mutant bound with ACE2 (bound state). For both kinds of systems,
185 mutation on one residue (E484K, N439K, K417N, T478I, P479S, S477N, N501Y) on RBD
186 (mutant systems) was conducted using VMD program [52]. After solvating the unbound systems
187 with enough amount of water and neutralizing them with 0.15M NaCl, and solvating the bound
188 system with the same amount of water and enough amount of ions on both the wildtype and mutant
189 systems, NAMD all-atom molecular dynamics simulations were performed to equilibrate both
190 kinds of systems using an NVT ensemble after a brief energy minimization. The dual-topology
191 methodology [65,66,67], and the soft-core potentials [68,69] were applied to overcome endpoint
192 singularities [70] in the FEP simulation, following the same method as in our previous work [50].
193 The free energy change in mutation for residue *i* in thermodynamic cycle can be calculated using
194 Equation (2):

195 $$\Delta G_{i,wildtype,bind} - \Delta G_{i,mutant,bind} = \Delta G_{i,unbound,alch} - \Delta G_{i,bound,alch} = \Delta\Delta G_i \quad (2)$$

196 Here, $\Delta\Delta G_i$ is the relative change of alchemical free energy of residue *i* during the binding of RBD
197 with ACE2 as the thermodynamic cycle shown in Figure S1. In each FEP simulation, 3 ns
198 simulations were performed in each window for both forward and backward directions and for
199 both the bound and free states after 0.5 ns simulations were conducted to equilibrate the system.
200 In this project, the interaction calculation includes 10 windows, ranging from a thermodynamic
201 coupling parameter λ values of zero to 1 (with a gap of 0.1) for a total of 20 simulations per
202 mutation. The time step was 1.0 fs.

203

204 ## Results

205 **1). RMSD, RMSF, ΔRMSF, DSSP results for ACE2 and RBD variants**

206 **RMSD result.** Based on all-atom NAMD simulations on different RBD variants bound with ACE2,
207 the RMSDs of the complex, RBD, ACE2 were calculated after aligning the trajectories to the RBD
208 wildtype bound with ACE2, RBD wildtype, and ACE2 individually. RBD mutants, ACE2, and the
209 complexes are very stable during 100 ns simulations and are very consistent with those from ACE2
210 bound with RBD wildtype (as the RMSD vs simulation time result shown in Figure S2 in SI).
211 Calculating the average RMSD of the complex, the RBD, and the ACE2, the results are shown in
212 Table 1. Only ACE2&RBD-N501Y complex has a RMSD (2.09±0.2Å) lower than that of the
213 ACE2&RBD wildtype(2.21±0.4Å). Although RBD-N501Y has the highest RMSD (1.54±0.1Å),
214 ACE2 bound with this RBD variant has the lowest RMSD (1.84±0.2Å). That suggests that RBD-
215 N501Y can fit the binding pocket of ACE2 with the minimum structure change on ACE2 and the
216 maximum structure adaptation of RBD-N501Y. On the other hand, the complexes of ACE2 with
217 RBD tri-mutant, RBD-T478I, and RBD-N439K showed the largest structural deviation from the
218 wildtype(3.05±0.4Å, 3.06±0.4Å, 3.34±0.5Å). When bound with RBD-N439K, ACE2 has the
219 largest structural deviation (2.60±0.3Å) comparing to the ACE2 wildtype (1.88±0.2Å). Overall,
220 the RMSD result suggests that spot mutation did not affect the binding structure of ACE2 with
221 RBD significantly.
222
223 Table 1. The average and standard deviations of RMSDs of ACE2&RBD complex, RBD wildtype
224 and variants, and ACE2, the number of hydrogen bonds (hbonds) formed, and the buried surface
225 area (BSA) between ACE2 and RBD. The standard deviations were calculated based on the
226 second-half of NAMD simulations.

Simulations	$RMSD_{Complex}$ (Å)	$RMSD_{RBD}$ (Å)	$RMSD_{ACE2}$ (Å)	Hbond	BSA ($Å^2$)

E484K&ACE2	2.40±0.3	1.22±0.1	1.92±0.1	2.63±1.7	864.3±57.4
N439K&ACE2	3.34±0.5	1.18±0.1	2.60±0.3	2.69±1.4	876.0±46.8
N501Y&ACE2	2.09±0.2	1.54±0.1	1.84±0.2	2.62±1.3	843.6±54.4
P479S&ACE2	2.74±0.7	1.21±0.1	2.11±0.2	3.23±1.5	861.0±62.0
K417N&ACE2	2.68±0.3	1.20±0.1	2.45±0.3	2.32±1.4	838.1±45.5
S477N&ACE2	2.89±0.4	1.15±0.1	2.50±0.2	3.03±1.4	908.6±41.4
T478I&ACE2	3.06±0.4	1.22±0.1	2.43±0.2	1.49±1.1	729.7±50.3
Tri-mutant&ACE2	3.05±0.4	1.32±0.2	2.10±0.2	2.01±1.2	835.5±46.5
RBD&ACE2 wt	2.21±0.4	1.23±0.1	1.88±0.2	2.64±1.4	863.3±44.4

RMSF and ΔRMSF result. Calculating the Root Mean Squared Fluctuation (RMSF) of RBD and ACE2 from different simulations, the results are shown in Figure 2(Left) and (Right). Residues from 455 to 505 on RBD bound with ACE2 at the region of RES19 to RES81, which are highlighted in light green for RBD on Figure 2(Left) and for ACE2 on Figure 2(Right). Within the binding region, all the mutants have a smaller RMSF than the wildtype, especially S477N, N439K, T478I and the tri-mutant. However, at other regions such as RES360 to RES390, E484K showed a larger structure fluctuation.

Figure 2. Comparison of RMSF from RBD variants and wildtype (Left) and ACE2 (Right). The variant results are shown in black solid line while the wildtype shown in red dashed line. The binding regions on RBD and ACE2 are shaded in light green, and the secondary structures of RBD and ACE2 are shown on the top of RMSF figures.

241 Mapping the change of RMSF ($\Delta RMSF=RMSF_{mutant}-RMSF_{wt}$) on the secondary structure of RBD
242 and ACE2, the result for N501Y is shown in Figure 3(Left) and the tri-mutant bound with ACE2
243 in Figure 3(Right). Comparing to the wildtype, RBD N501Y is slightly more rigid at RES501 site
244 and RES484 site, although other binding region has a similar rigidity to the free form. However,
245 ACE2 is more rigid on the binding interface except the loop region which becomes more flexible
246 than the ACE2 when bound with RBD wildtype. Figure 3(Right) shows that part of the binding
247 interface on RBD becomes more rigid, part unchanged while the left region become more flexible
248 comparing to the RBD wildtype, while ACE2 also has part of the interface more rigid, part
249 unchanged, and other part more flexible comparing to the ACE2 bound with RBD wildtype. Those
250 are consistent with RMSF result in Figure 2. Similarly, the ΔRMSF of other RBD mutants and
251 ACE2 were calculated and mapped to the secondary structure of RBD and ACE2 (shown in Figure
252 S3 to S5). In summary, the binding interface of ACE2 molecule becomes more rigid when bound
253 with RBD variants except with S477N and N439K which have more flexible region than rigid
254 region on the binding interface. Comparing to the RBD wildtype, RBD variants only become
255 slightly more rigid except RBD N439K variant which becomes mostly more flexible. Faraway
256 regions of ACE2 bound with RBD variants usually become more flexible (such as RBD-S477N,
257 RBD-N439K, and RBD-K417N, RBD-T478I), but not for the ACE2 bound with E484K, which
258 overall become more rigid. Those can agree with results in RMSF result shown in Figure 2, and
259 the result suggests that spot mutations on RBD can change the overall structure flexibility of RBD
260 and ACE2 comparing to the wildtype. Such kind of change of flexibility should contribute to the
261 adaptation of RBD variants to fit the binding pocket of ACE2 which also can adjust its flexibility
262 accordingly.
263

264 **Figure 3.** The ΔRMSF of RBD-N501Y and ACE2 (Left) from wildtype to variant forms of RBD
265 mapped to the initial bound structure of ACE2&RBD-N501Y; and the ΔRMSF of RBD-
266 trimutant and ACE2 (Right) mapped to its initial bound structure of the complex. Colors range
267 from blue to white to red (with white representing no change in RMSF, blue representing RMSF
268 decrease, and red representing RMSF increase). The ΔRMSF is in the range from -0.5 (totally
269 blue) to 0.5 (totally red).
270
271 **DSSP result.** In order to track the structure change of ACE2 and RBD contributed by the spot
272 mutation, the evolution of the secondary structure was predicted based on DSSP [71] calculation
273 over the simulation time using the wordom program. The DSSP program assigns the protein
274 secondary structure to one of the nine states defined, including three helix types (3_{10}, G; α, H; π,
275 I), two extended sheet types (antiparallel and parallel, E and X), two types of turns including the
276 helix turn (T) and β bridges (B), bend (S), and others (L). The secondary structure was calculated
277 for each residue at each time frame during the simulation time. Based on that, the average
278 proportion of helix (including G, H and I), sheet (including E), turn (including B and T) and other
279 (including X, S and L) structures on RBD and ACE2 over the simulation time were calculated,
280 and the results in comparison with available literature data [39] are shown in Figure 4 for RBD
281 and in Figure S6 in SI for ACE2.
282
283 **Figure 4.** Comparison of RBD DSSP with available literature data.
284
285 Overall, the proportions of RBD secondary structure elements are very consistent with available
286 experimental data [39], with around 13%-15% of helix, 30%-32% of sheet (including both parallel

287 and anti-parallel), and 13%-14% of turns, and 40%-43% of others. That implies the RBD structures
288 during NAMD simulations are reasonable. In Figure 4, comparing the RBD mutants with RBD
289 wildtype from the experimental data (the last 6 columns which only have RBD in free state
290 available), it shows that the average percentage of other structure is higher in RBD mutants than
291 the RBD wildtype. That is consistent with the simulation prediction for RBD wildtype and variants
292 (the first 9 columns which are all in bound form). That suggests that spot mutation can increase
293 undefined structure (other structure) in RBD. Although DSSP of RBD in wildtype free state (wt,
294 free) has similar helix and turn ratios to the experimental data of RBD in wildtype free state (wt,
295 free, ex), its sheet ratio is higher than the experimental data by around 6% while its other structure
296 ratio is lower than the experimental data by around 6%. Such kind of discrepancy should come
297 from the different definitions of sheet from Anderson [71] and the experimental method. Because
298 of that, the average percentage of sheet structure from simulations are overall higher than
299 experimental data while the average percentage of other structures are overall lower than
300 experimental data.
301 Comparing results from simulation only or from experiments only, overall spot mutation only
302 changes the secondary structure distribution of RBD slightly in both bound and free states. It
303 almost does not change the secondary structure distribution of ACE2 as shown in Figure S6. So,
304 overall, the mutants and wildtype have similar secondary structure distribution and spot mutation
305 should only affect the secondary structure locally.
306
307 **2). Hydrogen bonds formed on the binding interface**
308 Forming intermolecular hydrogen bonds is one of the major driving forces for the binding of RBD
309 with ACE2. Calculating the number of hydrogen bonds formed between ACE2 and RBD mutants

310 over the simulation time (shown in Figure S7), overall, RBD mutants formed similar amount of
311 hydrogen bonds with ACE2 to the RBD wildtype during the simulation time. Calculating the
312 average and standard deviation of the number of hydrogen bonds formed, the results are shown in
313 Table 1. S477N and P479S formed more hydrogen bonds with ACE2 than the wildtype, while
314 T478I formed the least, and the tri-mutant formed the second to the least amount of hydrogen
315 bonds with ACE2. Tracking the residues pairs on the binding interface, the results are shown in
316 Table S3 in SI. There are 8 pairs of residues forming hydrogen bonds on the RBD wildtype and
317 ACE2 interface, including Gly502-Lys353, Tyr505-Glu37, Asn487-Tyr83, Thr500-Tyr41,
318 Lys417-Asp30, Gln493-Glu35, Tyr449-Asp38, Gln498-Gln42. With the triple-mutation, three
319 pairs (Lys417-Asp30, Tyr449-Asp38, Gln498-Gln42) were broken and only the other five still
320 formed hydrogen bonds in the tri-mutant&ACE2 interface. However, a new hydrogen bond
321 formed between THR500-ASP355, and the interface structure generated from ligplot program [72]
322 in comparison with RBD wildtype are shown in Figure 5. The details of hydrogen bonds formed
323 between ACE2 and RBD wildtype and variants are shown in Table S3. Overall, similar binding
324 interface formed in RBD wt&ACE2 and RBD variant&ACE2, although the exact residues forming
325 hydrogen bonds changed and the number of hydrogen bonds formed also changed by certain
326 amount. Such kind of small modification on the binding interface contributes to the different
327 binding free energy of ACE2 and RBD which mainly comes from hydrogen bonds formation and
328 electrostatic and hydrophobic interactions [45], and affects the infectivity of CoV-2 variants.
329
330 **Figure 5**. Hydrogen bonds formed on the ACE2&RBD interface for the wildtype (Top) and tri-
331 mutant (Bottom) generated from ligplot program. Residues formed hydrogen bonds are connected

332 using dashed green lines. Residues on RBD are labelled in light green with bonds shown in
333 magenta, while residues on ACE2 are labelled in blue with bonds shown in orange.
334
335 **3). BSA and distance map result**
336 ***BSA comparison.*** Calculating the buried surface area (BSA) between ACE2 and RBD variants
337 over the simulation time, the results in comparison with the RBD wildtype are shown in Figure 6.
338 RBD wildtype and variants can bind with ACE2 consistently during the simulation time.
339 Calculating the average and standard deviations of BSA based on the second half of the simulation
340 time, the results are shown in Table 1. Overall, the RBD variants and ACE2 form a similar BSA
341 as the RBD wildtype and ACE2. The RBD-T478I formed a slightly smaller BSA than other
342 mutants, while RBD-E484K, RBD-N439K and RBD-S477N form a larger BSA with ACE2 than
343 the RBD wildtype; the RBD-trimutant forms the smallest BSA among all the simulations
344 especially during 20 to 100 ns period in the simulations as shown in Figure 6. Based on the findings
345 from Chan et al. [43], a larger BSA suggests a stronger binding of RBD with ACE2, thus it is
346 expected that E484K, N439K and S477N variants should form a stronger binding with ACE2 than
347 other variants, while the tri-mutant should form the less stable binding with ACE2.
348
349 **Figure 6.** Comparison of the BSA between RBD variants and ACE2 with that of the ACE2&RBD
350 wildtype started from the crystal structure.
351
352 **Distance map result comparison.** Calculating the distance map between residues on ACE2 and
353 RBD, the results of RBD-E484K bound with ACE2 in comparison with RBD wildtype bound with
354 ACE2 are shown in Figure 7 as an example. The other RBD variants bound with ACE2 distance

355 maps are shown in Figure S8 and S9 in SI. Those results show that different RBD variants bound
356 with ACE2 at the interface consistent with that of RBD wildtype and ACE2.
357 Even with the small modification on the residue pairs forming interactions on the binding interface,
358 a similar BSA and distance maps were formed for RBD variants with ACE2 comparing to RBD
359 wildtype. Thus it is not surprising to see that overall the binding structures of RBD mutants&ACE2
360 complexes are very consistent with the wildtype which is the crystal structure of RBD &ACE2
361 from Lan et al.[51], as the comparison of the initial and final structures for RBD-trimutant&ACE2
362 shown in Figure 1 (b). The structures of RBD mutants bound with ACE2 showed limited deviation
363 from the original structure, which can agree with RMSD, RMSF, BSA and hydrogen bonds results.
364
365
366 **Figure 7**. Distance map comparison of 1). RBD-E484K mutant bound with ACE2 and 2). RBD
367 wildtype bound with ACE2. The binding region (RES455 to 505) on RBD are highlighted in light
368 green. The color bars are shown on the right side of the distance maps, with a residue pair distance
369 being no larger than 4 Å shown in red, while a residue pair distance larger or equal to 14 Å shown
370 in white.
371
372 In summary, RBD-mutants bind with ACE2 consistently and at a consistent interface. Because the
373 spot mutation did not change the binding interface of RBD and ACE2 significantly, it is reasonable
374 to start from the crystal structure of ACE2&RBD to do FEP simulation and predict the spot
375 mutation effect on ΔΔG.
376 **4). FEP result**

377 Analyzing FEP simulation results, ΔΔG was predicted for RBD mutants. The results in comparison
378 with Upadhyay [39] are shown in Figure 8. The comparison of simulation prediction with three
379 more available literatures [34,35] are shown in Table 2.
380
381 **Figure 8**. ΔΔG for RBD variants binding with ACE2 predicted from FEP (shown in blue bars) in
382 comparison with literature data from Upadhyay et al. (shown in orange bars). Reference ΔΔG was
383 calculated based on available data in the table as $\Delta\Delta G=\Delta G_{mutant}-\Delta G_{wt.}$
384
385 Table 2. ΔΔG predicted from FEP in comparison with available literature data.

Mutants	FEP prediction (kcal/mol)	Upadhyay et al. (kcal/mol)	Luan et al. (kcal/mol)	Laffeber (kcal/mol)	Barton et al. (kcal/mol)
N501Y	-3.80±0.17	-0.70±0.40	-0.81	1.3	1.43±0.04
N439K	-2.26±0.20				
K417N	-0.56±0.21	1.30±0.10		-0.8	-0.96±0.06
E484K	0.36±0.27	0.90±0.10		0.2	0.20±0.04
S477N	-0.08±0.09	-0.40±0.20			0.33±0.04
P479S	0.58±0.07				
T478I	0.19±0.08	0.3±0.20			

386
387 Based on Figure 8, N501Y, N439K, K417N contribute to the binding of RBD with ACE2, T478I
388 and S477N have negligible effect, while neither E484K nor P479S contributes to the binding.
389 Upadhyay et al. [39] did ITC experiments on the binding of RBD mutants with ACE2. Calculating

390 $\Delta\Delta G$ using equation: $\Delta\Delta G=\Delta G_{mutant}-\Delta G_{wt}$ based on available data, $\Delta\Delta G$ data from Upadhyay are
391 shown in Figure 8 and Table 2 above. As can be seen from Upadhyay et al., N501Y can increase
392 the binding of RBD with ACE2, T478I has negligible effect while E484K can make the binding
393 weaker. Our prediction of those three mutations can agree with Upadhyay et al, and the effect of
394 N501Y also agrees with Luan et al. [41] who conducted all-atom molecular dynamics simulations
395 and FEP on RBD N501Y mutant binding with ACE2, and predicted the $\Delta\Delta G$=-0.81kcal/mol as
396 shown in Table 2.
397 However, FEP predicted that S477N should have negligible effect on RBD binding with ACE2,
398 while a stronger binding of RBD-S477N variant with ACE2 by Upadhyay et al. Although our
399 prediction deviated from Upadhyay et al, the effect of S477N from Upadhyay et al. was opposite
400 to the binding of RBD and ACE2 by Barton et al. The FEP prediction on K417N is opposite to
401 Upadhyay et al's work, although the FEP prediction can agree with the experimental work by
402 Laffeber et al [73] and Barton et al. [74] as shown in Table 2. The $\Delta\Delta G$ result from Laffeber et al.
403 [73] as shown were calculated after converting experimental data K_D for wildtype and mutants to
404 ΔG using the relationship as: $\Delta G_{exp}=-RT\ln K_D$ at T=298K.
405 N439K, which was found in multiple regions in the world and was a quite common mutation, can
406 enhance the binding of RBD with human ACE2 receptor while evade antibody mediated immunity
407 as found by Thomson et al. [37]. FEP predicted that N439K can decrease the binding free energy
408 of RBD with ACE2 thus should increase the binding affinity between them. Our prediction can
409 agree with Thomson et al.'s result [37].
410 Based on our FEP prediction, both N501Y and K417N can increase the binding affinity of RBD
411 and ACE2, but E484K has a negative effect on the binding. Because of that, the triple mutants of
412 K417A-E484A-N501A should contribute to the binding of RBD with ACE2 if assuming a linear

413 relationship between the effect of each mutation and the total effect. Because of that, it is expected
414 that ACE2 should bind with the triple mutant stronger than the wildtype. That agrees with the
415 infectivity of Beta variant. The FEP prediction on N501Y suggests that Alpha variant should be
416 more infectious than the original SARS-CoV-2. That also agrees with experimental and clinic
417 findings.
418
419 **4). Dihedral angle correlation covariance result**
420
421 In order to find out how spot mutations affect the dynamic correlation network of RBD, dihedral
422 angle ϕ, φ combined covariance matrix for RBD was calculated in both the wildtype and variant
423 forms, and in both bound and free states. The dihedral angle covariance matrices revealed a set of
424 highly correlated residues in RBD-N501Y and RBD-tri-mutant, as presented in Figure 9 (Left)
425 and (Right) individually. The RBD wildtype bound with ACE2 covariance matrix is shown in the
426 lower-right triangle below the diagonal line while the covariance matrices of RBD-N501Y variant
427 and tri-mutant variant are shown in the upper-left triangle above the diagonal line in both Figure
428 9 (Left) and (Right). RBD-N501Y variant lost the original correlation in RBD wildtype between
429 RES501 and other residues as pointed out by the orange arrows, but other correlations in the range
430 of RES470 to RES483 became stronger in RBD-N501Y variant (pointed out by red arrows) which
431 were weak in the original RBD wildtype. Another region around RES370 (pointed out by red
432 arrows) which is also faraway from RES501 site, shows a strong correlation in RBD-N501Y
433 variant, although such kind of strong correlation was not present in the RBD wildtype. Overall, a
434 stronger correlation shows up in RBD-N501Y variant comparing to the RBD wildtype. Similarly,
435 RBD-trimutant (three mutations as N501Y, E484K, K417N) (Figure 9(Right)) has more discrete
436 correlations (pointed out by red arrows) which were not originally in the RBD wildtype, while the

437 original correlations between N501, E484 and K417 and other residues (pointed out by orange
438 arrows) were lost. RES501 region in RBD-tri-mutant is strongly correlated with other regions as
439 pointed out by red arrows.
440
441 **Figure 9**. Comparison of the averaged mixed dihedral angle covariance matrix for RBD-N501Y (upper-
442 left triangle above the diagonal line) in comparison of RBD in wildtype (lower-right triangle) in bound state
443 (Left), and the averaged mixed dihedral angle covariance matrix for RBD-tri-mutation (upper-left triangle
444 above the diagonal line) in comparison of RBD in wildtype (Right). The color bars of covariance map are
445 shown on the right of the figures from blue to yellow corresponding to the covariance coefficient in the
446 range of -0.1 to 0.1. The secondary structure of RBD is shown on the top the covariance matrices, and the
447 residue numbers of RBD are labelled on both the x and y-axis.
448
449 **Figure 10**. Comparison of the averaged mixed dihedral angle covariance matrices for RBD-E484K (Left)
450 and RBD wildtype in free state (Right) (upper left triangle above the diagonal line) in comparison with
451 RBD wildtype in bound state (lower right). The color bars of covariance map are shown on the right of
452 the figures from blue to yellow corresponding to the covariance coefficient in the range of -0.1 to 0.1. The
453 secondary structure of RBD is shown on the top the covariance matrices, and the residue numbers of RBD
454 are labelled on both the x and y-axis.
455
456 The correlation matrices for RBD-E484K variant and RBD wildtype in free form were analyzed
457 with results in comparison with RBD wildtype in bound state shown in Figure 10 (Left) and (Right),
458 and results for other RBD variants in Figure S10 to S12. It was interesting to see that RBD-E484K
459 has strong correlation in the head (RES334-374) and tail (RES520-526) regions which are faraway
460 from each other, comparing to the RBD wildtype. The RBD wildtype in free state has a stronger
461 correlation at its tail region but weaker correlation at its head region than the RBD wildtype in

462 bound state. RES372 region has strong correlation with other residues. Since the RBD free state
463 simulation starts from the crystal structure of RBD (by removing the bound ACE2 in PDB ID of
464 6M0J) which is in open state, while binding of RBD with ligand can make the binding region more
465 rigid [47], that suggests that binding with ACE2 weakened the correlation of RBD in its tail region
466 which is the binding interface with ACE2.
467
468 **Figure 11**. Covariance coefficient between residue 373 (a)/residue 372 (b)/residue 480 (c) and
469 residue 501(d) and other residues mapped on the structure of RBD in the wildtype and bound state
470 (a), in the wildtype and free state (b), and in the N501Y variant (c), and in tri-mutant variant(d).
471 Positive covariance is shown in red while negative covariance in blue and the covariance equals to zero in
472 white. The range of covariance is in the range of -0.1 to 0.1. Residues have positive correlation with the
473 picked residue are labelled in red while in blue for negative correlation.
474
475 Similarly, other RBD variants have their correlation matrix changed comparing to the RBD
476 wildtype as results shown in Figure S10 to S12.
477
478 Since RES373 on RBD wildtype bound form, RES372 on RBD wildtype free form, RES480 on
479 RBD-N501Y, and RES501 on RBD-trimutant have strong correlation with other residues as shown
480 in Figure 9 and Figure 10, those residues were picked as base for RBD in different simulations
481 correspondingly. Mapping the covariance coefficients of the base residue with other residues on
482 the b-factor of the secondary structure of RBD, the results for RBD in wildtype bound form, in
483 wildtype free form, RBD-N501Y, RBD-trimutant are shown in Figure 11(a), (b), (c), and (d)
484 individually (The secondary structures mapped with covariance coefficients for other RBD
485 variants are not shown). In Figure 11, residues having a covariance coefficient higher than 0.05

486 were labelled, and in red for a positive correlation coefficient while in blue for a negative
487 correlation coefficient. Overall, RBD wildtype free form, RBD-N501Y, RBD-trimutant all have
488 more correlations than the RBD wildtype in bound form. In RBD-N501Y shown in Figure 11(c),
489 RES480 has strong correlation with P479, G476, F456, S469, N440, I441, T500, Y501, P507,
490 G485, H519, C525, G526, L335, N334. Besides that, other residues labelled in red and blue also
491 have correlation with E484. Checking all the secondary structures mapped with covariance
492 coefficients for RBD in different forms, some common correlations exist among residues, such as
493 RES366/363, RES373/372, RES402/403, RES440/441, RES443/444, RES465/464, RES475/476,
494 RES485/484, RES516/517, RES519, RES521/522, RES526/525 in different RBD covariance
495 matrices. That may suggest that mutating those residues will modify the dynamics network of RBD,
496 thus affect its binding with ACE2.
497
498 **Figure 12**. Community networks formed in the RBD-N501Y(Left), in wildtype bound form
499 (middle) and wildtype free form (Right) based on MD simulation and dynamical network
500 analysis. The RBD network structures are oriented in the same direction as the RBD shown in
501 Figure 1.
502
503 Because there are interactions inside the protein, the protein can be viewed as a network. Analyzing
504 the interaction inside the network, communication communities can be calculated. Using the plug-
505 in in the VMD 1.9.3 edition, the dynamical network in RBD wildtype and variants was analyzed
506 based on residue−residue interactions over time. The Cα atom in each residue was treated as one
507 node. Multiple nodes with strong interactions can form one community. It was found that usually
508 7 to 9 network communities formed in RBD in different forms and at different states. The results

for RBD-N501Y, RBD wildtype bound form, RBD wildtype free form are shown in Figure 12, and in Figure S13 to S14 for other RBD variants. Interestingly, the largest community (shown in blue) always extends from the tail region of RBD to the binding interface in the community maps. The largest community includes the following residues in common: RES335, RES348, RES373, RES428, RES437, RES471, RES490, RES493, RES495, RES496, RES516, RES519, RES521-526. Those residues are at the N-term, central, binding region, and tail of RBD.

Such kind of extensive community showed up in all other RBDs as their network community maps shown in Figure 12 and Figure S13 to S14. That suggests that there should be an intrinsic dynamic network community inside RBD distributed from the tail region to the central, and to the binding interface. Thus, the dynamics in RBD binding interface region should be transmitted to the tail of RBD thus to the other sections of S protein. It is expected that disrupting of this intrinsic network can affect the binding of RBD with ACE2 and with antibodies.

Discussion

Based on the findings from Chan et al. [43], a larger BSA suggests a stronger binding of RBD with ACE2, thus it is expected that E484K, N439K and S477N variants should form a stronger binding with ACE2 than other variants, while the tri-mutant should form a less stable binding with ACE2 based on results shown in Figure 6. However, those cannot agree with the $\Delta\Delta G$ result predicted from FEP as shown in Figure 8, which shows that N439K should decrease the binding free energy of RBD and ACE2, but not E484K. S477N almost does not change the binding free energy of RBD and ACE2. Thus, the size of BSA does not correlate to the binding affinity of RBD and ACE2 based on our test in this project.

532 Up to now, different results on spot mutation effects on the binding affinity of RBD with ACE2
533 were reported. Tian et al. [75] found that N501Y mutation can increase the binding affinity of
534 RBD with ACE2 receptor using both experimental and simulation methods, thus a higher rate of
535 transmission of SARS-CoV-2 variant. However, it was found that E484K did not contribute to the
536 binding of RBD with ACE2. That is different from Wang et al. [76], who found that E484K mutant
537 on RBD can increase the binding affinity of RBD with ACE2 receptor, while decreasing the
538 binding affinity of RBD with antibodies. Upadhyay et al. [39] found that mutants differ in their
539 expression levels. Of the eight best-expressed mutants, two (N501Y and K417T/E484K/N501Y)
540 showed stronger affinity to ACE2 compared with the wildtype, whereas four (Y453F, S477N,
541 T478I, and S494P) had similar affinity and two (K417N and E484K) had weaker affinity than the
542 wildtype. Compared with the wildtype, four mutants (K417N, Y453F, N501Y, and
543 K417T/E484K/N501Y) had weaker affinity for the CC12.1 antibody, whereas two (S477N and
544 S494P) had similar affinity, and two (T478I and E484K) had stronger affinity than the wildtype.
545 Mutants also differ in their thermal stability, with the two least stable mutants showing reduced
546 expression. Taken together, these results indicate that multiple factors contribute toward the
547 natural selection of variants, and all these factors need to be considered to understand the evolution
548 of the virus. In addition, since not all variants can escape a given neutralizing antibody, antibodies
549 to treat new variants can be chosen based on the specific mutations in that variant. Wang et al. [77]
550 indicated that T478I and N501Y substitutions were two S mutations important for receptor
551 adaption of SARS-CoV-2, potentially contributing to the spillover of the virus to many other
552 animal hosts. Therefore, more attention should be paid to SARS-CoV-2 variants with these two
553 mutations. In this project, it has been found that spot-mutation on RBD do not change the binding
554 interface between ACE2 and RBD comparing to the wildtype. However, each spot-mutation can

555 make different contributions to the binding free energy of RBD with ACE2. N501Y can increase
556 the binding of RBD with ACE2 significantly based on FEP prediction. That agrees with some
557 other researchers as shown in Table 2. Such kind of discrepancy emphasized the importance of
558 theoretical prediction and systematical comparative study on the SARS-CoV-2 spot-mutation
559 variants.
560 Based on the dihedral angle covariance matrix calculation, it was found that there are some
561 common correlations in RBD, no matter in variant or wildtype form, in bound or free state. Those
562 residues are mostly located in the largest network community predicted by dynamic network
563 analysis with results shown in Figure 12 and Figure S13 to S14. Since the community is intrinsic
564 in RBD, and it extends from tail region of RBD to the binding interface region, it is expected that
565 mutation on those results can affect the binding of RBD with ACE2 and with antibodies.
566 Since the spike protein of SARS-CoV-2 is a trimer and each monomer has more than 1000 residues
567 [78], more work should be done in order to understand how the spot mutations on S protein affect
568 its structure, dynamics and function thus to supply insight on designing novel drugs against future
569 pandemic.
570
571
572 **Conclusions**
573
574 In this project, all-atom molecular dynamics simulations using NAMD program were conducted
575 on seven RBD single mutants and one RBD triple mutant binding with ACE2. It was found that
576 spot mutations on RBD do not affect the binding interface of RBD with ACE2 significantly.
577 Similar number of hydrogen bonds are still formed on the binding interface between RBD and

578 ACE2 after spot mutation, although some of the exact residues forming hydrogen bonds changed.
579 The distance map result shows that RBD mutant and ACE2 form the binding interface consistent
580 with the RBD wildtype, and they also form a similar buried surface area on the interface. Thus,
581 the structures of RBD mutants bound with ACE2 are very consistent with RBD wildtype with
582 ACE2. Calculating ΔΔG of spot mutation using FEP method, it was found that N501Y, N439K,
583 K417N can improve the binding of RBD with ACE2; E484K and P479S could not increase the
584 binding of RBD with ACE2; S477N and T478I do not affect the binding of RBD with ACE2. The
585 spot mutation changed the dynamic correlation network of residues on RBD based on the dihedral
586 correlation calculation, but an intrinsic network community exists in RBD which extends from the
587 tail region to the central region, then to the binding interface region. The result in this project can
588 supply the methodology and molecular insight on studying the molecular structure and dynamics
589 of possible future pandemics and design novel drugs.
590

591 ## Acknowledgements

592 This work was supported by National Science Foundation (NSF) Grant NO. 2200138. The
593 simulations were performed using supercomputer time from XSEDE via an award to Zhang L.
594 (MCB160041), and with some trajectory analysis partially using the high performance computers
595 at UTC, and one simulation performed on Unity computers of URI.
596

597 **References**:

1. WHO (2021) Coronavirus (COVID-19) dashboard Accessed March 22, 2023. Webpage: https://www.who.int/emergencies/diseases/novel-coronavirus-2019.

2. Siu YL, Teoh KT, Lo J, Chan CM, Kien F, Escriou N, Tsao SW, Nicholls JM, Altmeyer R, Peiris J SM, Bruzzone R, Nal B. The M, E, and N structural proteins of the severe acute respiratory syndrome

coronavirus are required for efficient assembly, trafficking, and release of virus-like particles. J Virol. 2008; 82:11318-11330.

3. Yoshimoto FK. The Proteins of Severe Acute Respiratory Syndrome Coronavirus-2 (SARS CoV-2 or n-COV19), the Cause of COVID-19. Protein J. 2020; 39:198-216.

4. Walls AC, Tortorici MA, Bosch B-J, Frenz B, Rottier PJM, DiMaio F, Rey FA, Veesler D. Cryo-electron microscopy structure of a coronavirus spike glycoprotein trimer. Nature. 2016; 531:114-117.

5. Wrapp D, Wang N, Corbett KS, Goldsmith JA, Hsieh C-L, Abiona O, Graham BS, McLellan JS. Cryo-EM structure of the 2019-nCoV spike in the prefusion conformation. Science. 2020; 367:1260-1263.

6. Walls AC, Park Y-J, Tortorici MA, Wall A, McGuire AT, Veesler D. Structure, Function, and Antigenicity of the SARS-CoV-2 Spike Glycoprotein. Cell. 2020; 181: 281-292.e286.

7. Yan R, Zhang Y, Li Y, Xia L, Guo Y, Zhou Q. Structural basis for the recognition of SARS-CoV-2 by full-length human ACE2. Science. 2020; 367: 1444-1448.

8. Lan J, Ge J, Yu J, Shan S, Zhou H, Fan S, Zhang Q, Shi X, Wang Q, Zhang L, Wang X. Structure of the SARS-CoV-2 spike receptor-binding domain bound to the ACE2 receptor. Nature. 2020; 581: 215-220.

9. McCallum M, Walls AC, Bowen JE, Corti D, Veesler D. Structure-guided covalent stabilization of coronavirus spike glycoprotein trimers in the closed conformation. Nat Struct Mol Biol. 2020; 27: 942–949.

10. Masters PS. The molecular biology of coronaviruses. Adv. Virus Res. 2006; 66: 193–292.

11. Davies NG, Abbott S, Barnard RC, Jarvis CI, Kucharski AJ, Munday JD, Pearson CAB, Russell TW, Tully DC, Washburne AD, Wenseleers T, Gimma A, Waites W, Wong KLM, van Zandvoort K, Silverman JD, CMMID COVID-19 Working Group, COVID-19 Genomics UK (COG-UK) Consortium, Diaz-Ordaz K, Keogh R, Eggo RM, Funk S, Jit M, Atkins KE, Edmunds WJ. Estimated transmissibility and impact of SARS-COV-2 lineage b.1.1.7 in England. Science. 2021; 372: abg3055.

12. Korber B, Fischer WM, Gnanakaran S, Yoon H, Theiler J, Abfalterer W, Hengartner N, Giorgi EE, Bhattacharya T, Foley B, Hastie KM, Parker MD, Partridge DG, Evans CM, Freeman TM, de Silva TI,

13. Volz E, Hill V, McCrone JT, Price A, Jorgensen D, O'Toole Á, Southgate J, Johnson R, Jackson B, Nascimento FF, Rey SM, Nicholls SM, Colquhoun RM, da Silva Filipe A, Shepherd J, Pascall DJ, Shah R, Jesudason N, Li K, Jarrett R, Pacchiarini N, Bull M, Geidelberg L, Siveroni I, COG-UK Consortium, Goodfellow I, Loman NJ, Pybus OG, Robertson DL, Thomson EC, Rambaut A, Connor TR. Evaluating the effects of SARS-COV-2 spike mutation D614G on transmissibility and pathogenicity. Cell. 2021b; 184: 64–75.

14. Washington NL, Gangavarapu K, Zeller M, Bolze A, Cirulli ET, Schiabor Barrett KM, Larsen BB, Anderson C, White S, Cassens T, Jacobs S, Levan G, Nguyen J, Ramirez JM, Rivera-Garcia C, Sandoval E, Wang X, Wong D, Spencer E, Robles-Sikisaka R, Kurzban E, Hughes LD, Deng X, Wang C, Servellita V, Valentine H, De Hoff P, Seaver P, Sathe S, Gietzen K, Sickler B, Antico J, Hoon K, Liu J, Harding A, Bakhtar O, Basler T, Austin B, MacCannell D, Isaksson M, Febbo PG, Becker D, Laurent M, McDonald E, Yeo GW, Knight R, Laurent LC, de Feo E, Worobey M, Chiu CY, Suchard MA, Lu JT, Lee W, Andersen KG. Emergence and rapid transmission of SARS-COV-2 b.1.1.7 in the United States. Cell. 2021; 184: 2587–2594.

15. Darby AC, Hiscox JA. Covid-19: Variants and vaccination. BMJ. 2021; 372: n771.

16. Dejnirattisai W, Zhou D, Supasa P, Liu C, Mentzer AJ, Ginn HM, Zhao Y, Duyvesteyn HME, Tuekprakhon A, Nutalai R, Wang B, López-Camacho C, Slon-Campos J, Walter TS, Skelly D, Costa Clemens SA, Naveca FG, Nascimento V, Nascimento F, Fernandes da Costa C, Resende PC, Pauvolid-Correa A, Siqueira MM, Dold C, Levin R, Dong T, Pollard AJ, Knight JC, Crook D, Lambe T, Clutterbuck E, Bibi S, Flaxman A, Bittaye M, Belij-Rammerstorfer S, Gilbert SC, Carroll MW, Klenerman P, Barnes E, Dunachie SJ, Paterson NG, Williams MA, Hall DR, Hulswit RJG, Bowden TA, Fry EE, Mongkolsapaya

Sheffield COVID-19 Genomics Group, McDanal C, Perez LG, Tang H, Moon-Walker A, Whelan SP, LaBranche CC, Saphire EO, Montefiori DC. Tracking changes in sars-cov-2 spike: Evidence that d614g increases infectivity of the COVID-19 virus. Cell. 2020; 182: 812–827.

J, Ren J, Stuart DI, Screaton GR. Antibody evasion by the p.1 strain of SARS-COV-2. Cell. 2021; 184: 2939–2954.

17. Garcia-Beltran WF, Lam EC, KSt D, Nitido AD, Garcia ZH, Hauser BM, Feldman J, Pavlovic MN, Gregory DJ, Poznansky MC, Sigal A, Schmidt AG, Iafrate AJ, Naranbhai V, Balazs AB. Multiple SARS-CoV-2 variants escape neutralization by vaccine-induced humoral immunity. Cell. 2021; 184: 2372–2383.

18. Madhi SA, Izu A, Pollard AJ. ChAdOx1 nCoV-19 Vaccine Efficacy against the B.1.351 Variant. The New England Journal of Medicine. 2021a; 385: 571–572.

19. Madhi SA, Baillie V, Cutland CL, Voysey M, Koen AL, Fairlie L, Padayachee SD, Dheda K, Barnabas SL, Bhorat QE, Briner C, Kwatra G, Ahmed K, Aley P, Bhikha S, Bhiman JN, Bhorat AE, du PJ, Esmail A, Groenewald M, Horne E, Hwa SH, Jose A, Lambe T, Laubscher M, Malahleha M, Masenya M, Masilela M, McKenzie S, Molapo K, Moultrie A, Oelofse S, Patel F, Pillay S, Rhead S, Rodel H, Rossouw L, Taoushanis C, Tegally H, Thombrayil A, van ES, Wibmer CK, Durham NM, Kelly EJ, Villafana TL, Gilbert S, Pollard AJ, de OT, Moore PL, Sigal A, Izu A. Safety and Efficacy of the Chadox1 NCOV-19 (AZD1222) Covid-19 Vaccine against the b.1.351 Variant in South Africa. medRxiv. 2021b.

20. Mahase E. Covid-19: Where are we on vaccines and variants. BMJ. 2021; 372: n597.

21. Davies N. G., Abbott S., Barnard R.C., Jarvis C.I., Kucharski A.J., Munday J.D., Pearson C.A.B, Russell T.W., Tully D.C., Washburne A.D., et al. Estimated transmissibility and impact of SARS-CoV-2 lineage B.1.1.7 in England. Science. 2021; 372: eabg3055. doi: 10.1126/science.abg3055.

22. Tegally H., Wilkinson E., Giovanetti M., Iranzadeh A., Fonseca V., Giandhari J., Doolabh D., Pillay S., San E.J., Msomi N., et al. Detection of a SARS-CoV-2 variant of concern in South Africa. Nature. 2021; 592: 438–443. doi: 10.1038/s41586-021-03402-9.

23. Faria N.R., Mellan T.A., Whittaker C., Claro I. M., Candido D.d.S., Mishra S., Crispim M.A.E., Sales F.C.S., Hawryluk I., McCrone J.T., et al. Genomics and epidemiology of the P.1 SARS-CoV-2 lineage in Manaus,Brazil. Science. 2021; 372: 815–821. doi: 10.1126/science.abh2644.

24. Fontanet A., Autran B., Lina B., Kieny M.P., Karim S.S.A, Sridhar D.J.T.L. SARS-CoV-2 variants and ending the COVID-19 pandemic. Lancet. 2021; 397: 952–954. doi: 10.1016/S0140-6736(21)00370-6.

25. Kannan S.R., Spratt A.N., Cohen A.R., Naqvi S.H., Chand H.S., Quinn T.P., Lorson C.L., Byrareddy S.N., Singh K. Evolutionary analysis of the Delta and Delta Plus variants of the SARS-CoV-2 viruses. J. Autoimmun. 2021; 124: 102715. doi: 10.1016/j.jaut.2021.102715.

26. Torjesen I. COVID-19: Omicron may be more transmissible than other variants and partly resistant to existing vaccines, scientists fear. BMJ. 2021; 375: n2943. doi: 10.1136/bmj.n2943.

27. Gao S.J., Guo H., Luo G. Omicron variant (B.1.1.529) of SARS-CoV-2, a global urgent public health alert! J. Med. Virol. 2021; 94: 1255–1256. doi: 10.1002/jmv.27491.

28. Han P., Li L., Liu S., Wang Q., Zhang D., Xu Z., Han P., Li X., Peng Q., Su C., et al. Receptor binding and complex structures of human ACE2 to spike RBD from omicron and delta SARS-CoV-2. Cell. 2022; 185: 630–640.e10. doi: 10.1016/j.cell.2022.01.001.

29. Chen J, Wang R, Wang M, Wei GW. Mutations Strengthened SARS-CoV-2 Infectivity. J Mol Biol. 2020; 432(19): 5212-5226. doi: 10.1016/j.jmb.2020.07.009.

30. Starr TN, Greaney AJ, Hilton SK, Ellis D, Crawford KHD, Dingens AS, Navarro MJ, Bowen JE, Tortorici MA, Walls AC, King NP, Veesler D, Bloom JD. Deep mutational scanning of SARS-COV-2 receptor binding domain reveals constraints on folding and ace2 binding. Cell. 2020; 182: 1295–1310.

31. Supasa P, Zhou D, Dejnirattisai W, Liu C, Mentzer AJ, Ginn HM, Zhao Y, Duyvesteyn HME, Nutalai R, Tuekprakhon A, Wang B, Paesen GC, Slon-Campos J, López-Camacho C, Hallis B, Coombes N, Bewley KR, Charlton S, Walter TS, Barnes E, Dunachie SJ, Skelly D, Lumley SF, Baker N, Shaik I, Humphries HE, Godwin K, Gent N, Sienkiewicz A, Dold C, Levin R, Dong T, Pollard AJ, Knight JC, Klenerman P, Crook D, Lambe T, Clutterbuck E, Bibi S, Flaxman A, Bittaye M, Belij-Rammerstorfer S, Gilbert S, Hall DR, Williams MA, Paterson NG, James W, Carroll MW, Fry EE, Mongkolsapaya J, Ren J, Stuart DI, Screaton GR. Reduced neutralization of SARS-COV-2 b.1.1.7 variant by convalescent and vaccine Sera. Cell. 2021; 184: 2201–2211.

32. Xie X., Liu Y., Liu J., et al. Neutralization of SARS-CoV-2 spike 69/70 deletion, E484K and N501Y variants by BNT162b2 vaccine-elicited sera. Nat Med. 2021; 27: 620–621. https://doi.org/10.1038/s41591-021-01270-4.

33. Wang WB, Liang Y, Jin YQ, Zhang J, Su JG, Li QM. E484K mutation in SARS-CoV-2 RBD enhances binding affinity with hACE2 but reduces interactions with neutralizing antibodies and nanobodies: Binding free energy calculation studies. J Mol Graph Model. 2021; 109: 108035. doi: 10.1016/j.jmgm.2021.108035. Epub 2021 Sep 17. PMID: 34562851; PMCID: PMC8447841.

34. Nelson G, Buzko O, Spilman P, Niazi K, Rabizadeh S, Soon-Shiong P. Molecular dynamic simulation reveals E484K mutation enhances spike RBD-ACE2 affinity and the combination of E484K, K417N and N501Y mutations (501Y.V2 variant) induces conformational change greater than N501Y mutant alone, potentially resulting in an escape mutant. bioRxiv 2021.01.13.426558; doi: https://doi.org/10.1101/2021.01.13.426558.

35. Barton MI, MacGowan SA, Kutuzov MA, Dushek O, Barton GJ, van der Merwe PA. Effects of common mutations in the SARS-CoV-2 Spike RBD and its ligand, the human ACE2 receptor on binding affinity and kinetics. Elife. 2021;10: e70658. doi: 10.7554/eLife.70658. PMID: 34435953; PMCID: PMC8480977.

36. Wang Z., Schmidt F., Weisblum Y., et al. mRNA vaccine-elicited antibodies to SARS-CoV-2 and circulating variants. Nature. 2021; 592: 616–622.

37. Thomson EC, Rosen LE, Shepherd JG, Spreafico R, da Silva Filipe A, Wojcechowskyj JA, Davis C, Piccoli L, Pascall DJ, Dillen J, Lytras S, Czudnochowski N, Shah R, Meury M, Jesudason N, De Marco A, Li K, Bassi J, O'Toole A, Pinto D, Colquhoun RM, Culap K, Jackson B, Zatta F, Rambaut A, Jaconi S, Sreenu VB, Nix J, Zhang I, Jarrett RF, Glass WG, Beltramello M, Nomikou K, Pizzuto M, Tong L, Cameroni E, Croll TI, Johnson N, Di Iulio J, Wickenhagen A, Ceschi A, Harbison AM, Mair D, Ferrari P, Smollett K, Sallusto F, Carmichael S, Garzoni C, Nichols J, Galli M, Hughes J, Riva A, Ho A, Schiuma M, Semple MG, Openshaw PJM, Fadda E, Baillie JK, Chodera JD; ISARIC4C Investigators; COVID-19 Genomics UK (COG-UK) Consortium; Rihn SJ, Lycett SJ, Virgin HW, Telenti A, Corti D, Robertson DL,

Snell G. Circulating SARS-CoV-2 spike N439K variants maintain fitness while evading antibody-mediated immunity. Cell. 2021; 184(5): 1171-1187.e20. doi: 10.1016/j.cell.2021.01.037.

38. Shu Y., McCauley J. GISAID: Globalinitiative on sharing all influenza data–from vision to reality. Eurosurveillance. 2017; 22(13).

39. Upadhyay V, Lucas A, Panja S, Miyauchi R, Mallela KMG. Receptor binding, immune escape, and protein stability direct the natural selection of SARS-CoV-2 variants. J Biol Chem. 2021; 297(4): 101208. doi: 10.1016/j.jbc.2021.101208. Epub 2021 Sep 17. PMID: 34543625; PMCID: PMC8445900.

40. Alaofi A. L., Shahid M. Mutations of SARS-CoV-2 RBD May Alter Its Molecular Structure to Improve Its Infection Efficiency. Biomolecules. 2021; 11: 1273. doi:10.3390/biom11091273.

41. Luan B, Wang H, Huynh T. Enhanced binding of the N501Y-mutated SARS-CoV-2 spike protein to the human ACE2 receptor: insights from molecular dynamics simulations. FEBS Lett. 2021; 595(10):1454-1461. doi: 10.1002/1873-3468.14076. Epub 2021 Apr 3. PMID: 33728680; PMCID: PMC8250610.

42. Kodchakorn K., Kongtawelert P. Molecular dynamics study on the strengthening behavior of Delta and Omicron SARS-CoV-2 spike RBD improved receptor-binding affinity. PloS one. 2022; 17(11): e0277745. doi:10.1371/journal.pone.0277745.

43. Chan KC, Song Y, Xu Z, Shang C, Zhou R. SARS-CoV-2 Delta Variant: Interplay between Individual Mutations and Their Allosteric Synergy. Biomolecules. 2022; 12(12): 1742. https://doi.org/10.3390/biom12121742.

44. Kim S, Liu Y, Ziarnik M, Seo S, Cao Y, Zhang XF, Im W. Binding of human ACE2 and RBD of Omicron enhanced by unique interaction patterns among SARS-CoV-2 variants of concern. Journal of Computational Chemistry. 2023; 44: 594-601.

45. Jawad B, Adhikari P, Podgornik R, Ching W. Key Interacting Residues between RBD of SARS-CoV-2 and ACE2 Receptor: Combination of Molecular Dynamics Simulation and Density Functional Calculation. J. Chem. Inf. Model. 2021; 61(9): 4425–4441.

46. Dutta S, Panthi B, Chandra A. All-Atom Simulations of Human ACE2-Spike Protein RBD Complexes for SARS-CoV-2 and Some of its Variants: Nature of Interactions and Free Energy Diagrams for Dissociation of the Protein Complexes. The journal of physical chemistry. B. 2022; 126(29): 5375–5389. https://doi.org/10.1021/acs.jpcb.2c00833.

47. Zhang L, Ghosh S K, Basavarajappa S C, Muller-Greven J, Penfield J, Brewer A, Ramakrishnan P, Buck M, Weinberg A. HBD-2 binds SARS-CoV-2 RBD and blocks viral entry: Strategy to combat COVID-19. iScience. 2022; 25: 103856.

48. Luan B, Huynh T. In Silico Antibody Mutagenesis for Optimizing Its Binding to Spike Protein of Severe Acute Respiratory Syndrome Coronavirus 2. J. Phys. Chem. Lett. 2020; 11: 9781-9787. doi:10.1021/acs.jpclett.0c02706.

49. Li Z, Zhang J Z H. Mutational Effect of Some Major COVID-19 Variants on Binding of the S Protein to ACE2. Biomolecules. 2022; 12: 572. doi:10.3390/biom12040572.

50. Brewer A, Zhang L. Binding Free Energy Calculation on Human Beta Defensin 3 on Negatively Charged Lipid Bilayer Using Free Energy Perturbation Method. Biophysical Chemistry. 2021; 277: 106662.

51. Lan J, Ge J, Yu J, et al. Structure of the SARS-CoV-2 spike receptor-binding domain bound to the ACE2 receptor. Nature. 2020; 581: 215–220. https://doi.org/10.1038/s41586-020-2180-5.

52. Humphrey W, Dalke A, Schulten K. VMD: visual molecular dynamics. J Mol Graph. 1996; 14: 33-38, 27-38.

53. Huang J, Rauscher S, Nawrocki G, Ran T, Feig M, de Groot BL, Grubmüller H, MacKerell, A.D. Jr. CHARMM36m: an improved force field for folded and intrinsically disordered proteins. Nat Methods. 2017; 14: 71-73.

54. Phillips JC, Braun R, Wang W, Gumbart J, Tajkhorshid E, Villa E, Chipot C, Skeel RD, Kalé L, Schulten K. Scalable molecular dynamics with NAMD. J Comput Chem. 2005; 26(16):1781-802. doi: 10.1002/jcc.20289. PMID: 16222654; PMCID: PMC2486339.

55. Huang J, Rauscher S, Nawrocki G, Ran T, Feig M, de Groot BL, Grubmüller H, MacKerell Jr. AD. CHARMM36m: an improved force field for folded and intrinsically disordered proteins. Nat Methods. 2017; 14(1): 71-73. doi: 10.1038/nmeth.4067. Epub 2016 Nov 7. PMID: 27819658; PMCID: PMC5199616.

56. Seeber M, Cecchini M, Rao F, Settanni G, Caflisch A. Wordom: a program for efficient analysis of molecular dynamics simulations. Bioinformatics. 2007; 23: 2625-2627.

57. Seeber M, Felline A, Raimondi F, Muff S, Friedman R, Rao F, ..., Fanelli F. Wordom: a user-friendly program for the analysis of molecular structures, trajectories, and free energy surfaces. J. Comput. Chem. 2011; 32:1183-1194.

58. Fisher N I, Lee A J. A Correlation Coefficient for Circular Data. Biometrika. 1983; 70: 327−332.

59. Fisher N. I. Statistical Analysis of Circular Data. Cambridge University Press: New York, 1993, p 277.

60. Mardia K V, Jupp P E. Directional Statistics. Wiley: Chichester, UK, 2000, p 429.

61. Zhang L, Buck M. Molecular Dynamics Simulations Reveal Isoform Specific Contact Dynamics Between the Plexin Rho GTPase Binding Domain (RBD) and Small Rho GTPases Rac1 and Rnd1. J. Phys. Chem. B. 2017; 121: 1485–1498.

62. Zhang L, Centa T, Buck M. Structure and dynamics analysis on plexin-B1 Rho-GTPase binding domain monomer and dimer. J. Phys. Chem. B. 2014; 118: 7302–11.

63. Sethi A, Eargle J, Black A, Luthey-Schulten Z. Dynamical Networks in tRNA:protein Complexes. Proc. Natl. Acad. Sci. U.S.A. 2009; 106: 6620−6625.

64. Glykos N. Software News and Updates. Carma: a Molecular Dynamics Analysis Program. J. Comput. Chem. 2006; 27: 1765−1768.

65. Frenkel D, Smit B. Understanding Molecular Simulation (Academic Press, San Diego). 2nd Ed. 2002.

66. Kirkwood J G. “Statistical mechanics of fluid mixtures”. J Chem Phys. 1935; 3: 300–313.

67. Straatsma T P, McCammon J A. Multiconfiguration thermodynamic integration. J Chem Phys. 1991; 95: 1175–1188.

68. Zacharias M, Straatsma T P, McCammon J A. Separation-shifted scaling, a new scaling method for Lennard-Jones interactions in thermodynamic integration, J. Chem. Phys. 1994; 100, 9025.

69. Beutler T C, Mark A E, van Schaik R C, Gerber P R, van Gunsteren W F. Avoiding singularities and numerical instabilities in free energy calculations based on molecular simulations. Chem. Phys. Lett. 1994; 222: 529–539.

70. Pohorille A, Jarzynski C, Chipot C. Good practices in free-energy calculations. J Phys. Chem. B. 2010; 114: 10235–10253.

71. Andersen C A F, Palmer A G, Brunak S, Rost B. Continuum secondary structure captures protein flexibility. Structure. 2002; 10(2):175-84. doi: 10.1016/s0969-2126(02)00700-1.

72. Laskowski R A, Swindells M B. LigPlot+: multiple ligand-protein interaction diagrams for drug discovery. J. Chem. Inf. Model. 2011; 51: 2778-2786.

73. Laffeber C, Koning K de, Kanaar R, Lebbink JHG. Experimental Evidence for Enhanced Receptor Binding by Rapidly Spreading SARS-CoV-2 Variants. J Mol Biol. 2021; 433(15):167058. doi: 10.1016/j.jmb.2021.167058. Epub 2021 May 21. PMID: 34023401; PMCID: PMC8139174.

74. Barton MI, MacGowan SA, Kutuzov MA, Dushek O, Barton GJ, van der Merwe PA. Effects of common mutations in the SARS-CoV-2 Spike RBD and its ligand, the human ACE2 receptor on binding affinity and kinetics. Elife. 2021; 10:e70658. doi: 10.7554/eLife.70658. PMID: 34435953; PMCID: PMC8480977.

75. Tian F, Tong B, Sun L, Shi S, Zheng B, Wang Z, Dong X, Zheng P. N501Y mutation of spike protein in SARS-CoV-2 strengthens its binding to receptor ACE2. eLife. 2021; 10: e69091.

76. Wang WB, Liang Y, Jin YQ, Zhang J, Su JG, Li QM. E484K mutation in SARS-CoV-2 RBD enhances binding affinity with hACE2 but reduces interactions with neutralizing antibodies and nanobodies: Binding free energy calculation studies. J Mol Graph Model. 2021; 109:108035.

77. Wang Q, Ye S B, Zhou Z J, Li J Y, Lv J Z, Hu B, Yuan S, Qiu Y, Ge X Y. Key mutations on spike protein altering ACE2 receptor utilization and potentially expanding host range of emerging SARS-CoV-2 variants. J Med Virol. 2022; 95(1): e28116. https://doi.org/10.1002/jmv.28116.

78. Xu C, Wang Y, Liu C, Zhang C, Han W, Hong X, Wang Y, Hong Q, Wang S, Zhao Q, Wang Y, Yang Y, Chen K, Zheng W, Kong L, Wang F, Zuo Q, Huang Z, Cong Y. Conformational dynamics of SARS-CoV-2 trimeric spike glycoprotein in complex with receptor ACE2 revealed by cryo-EM. Science advances. 2021; 7(1): eabe5575. doi:10.1126/sciadv.abe5575.

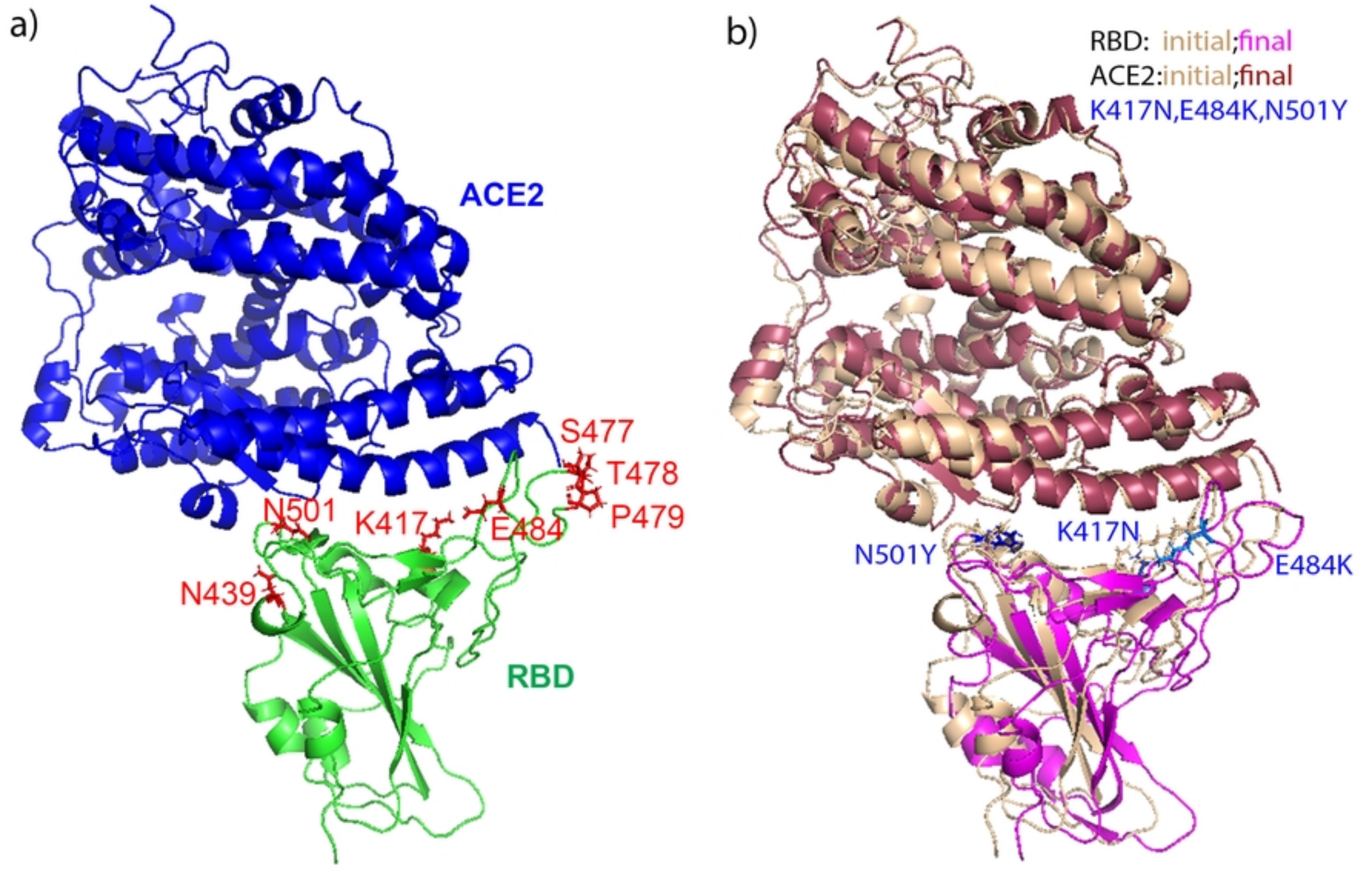
a)
ACE2
S477
T478
P479
N501
K417
E484
N439
RBD
b)
RBD: initial;final
ACE2:initial;final
K417N,E484K,N501Y
N501Y
K417N
E484K

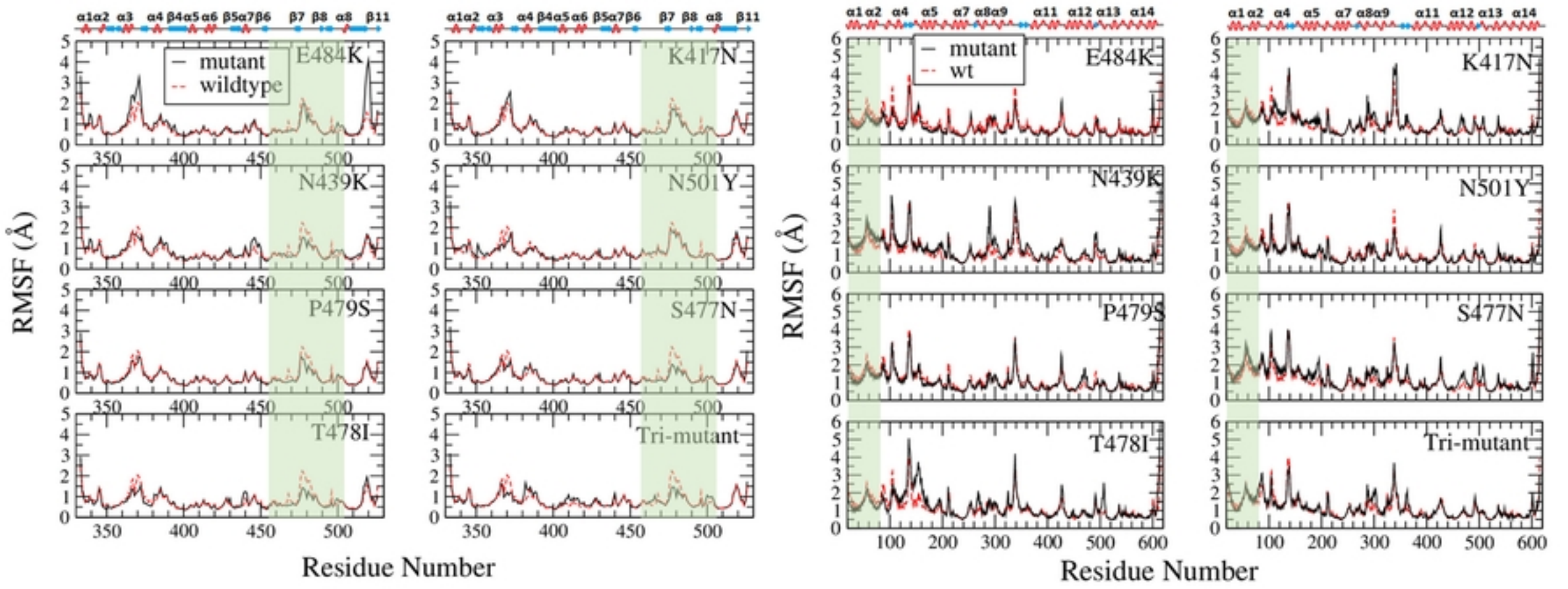
α1α2 α3 α4 β4α5α6 β5α7β6 β7 β8 α8 β11
mutant
wildtype
E484K
K417N
N439K
N501Y
P479S
S477N
T478I
Tri-mutant
RMSF (Å)
Residue Number
α1 α2 α4 α5 α7 α8α9 α11 α12 α13 α14
mutant
wt
E484K
K417N
N439K
N501Y
P479S
S477N
T478I
Tri-mutant
RMSF (Å)
Residue Number

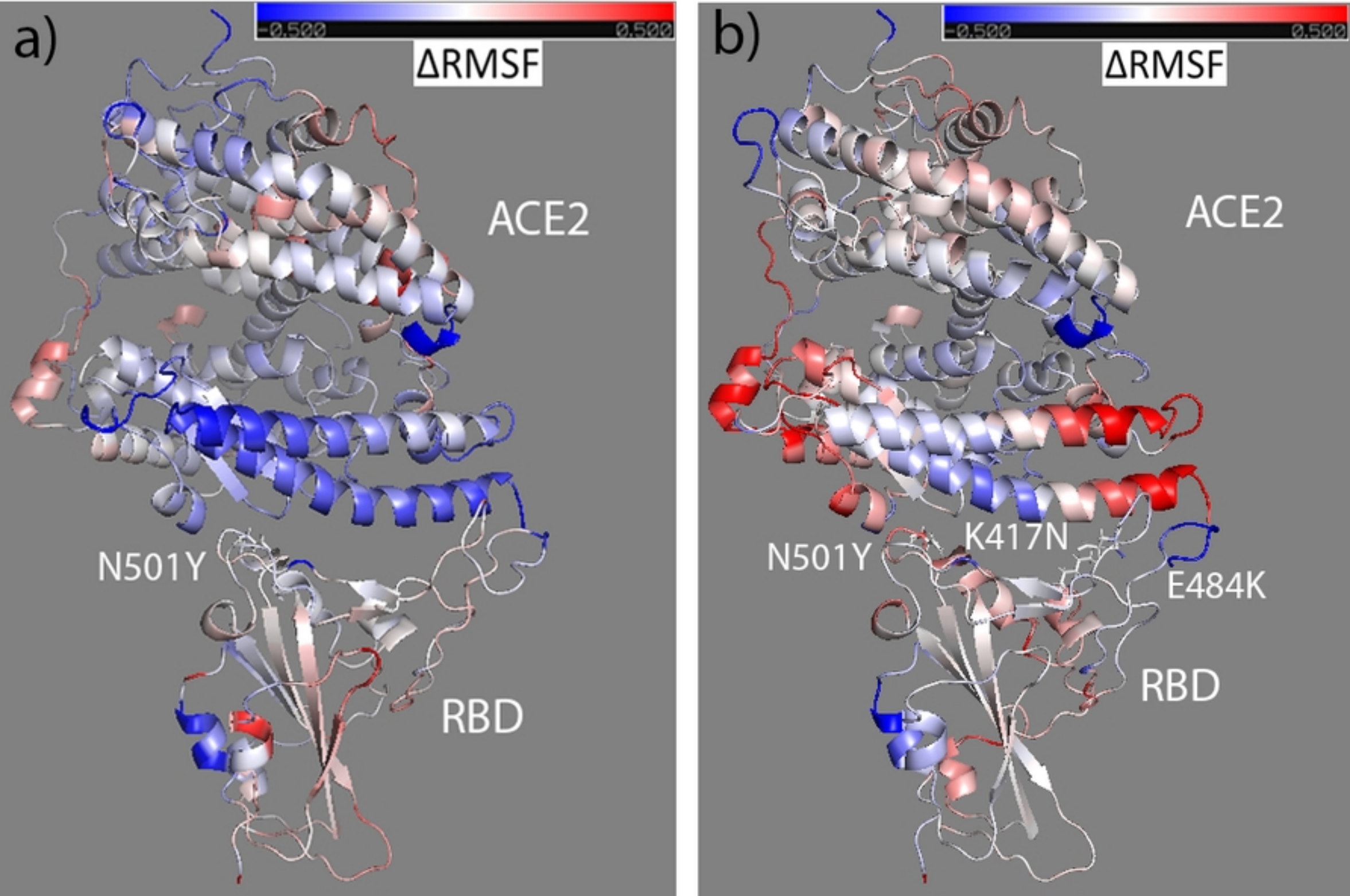
a)
-0.500
0.500
ΔRMSF
ACE2
N501Y
RBD
b)
-0.500
0.500
ΔRMSF
ACE2
N501Y
K417N
E484K
RBD

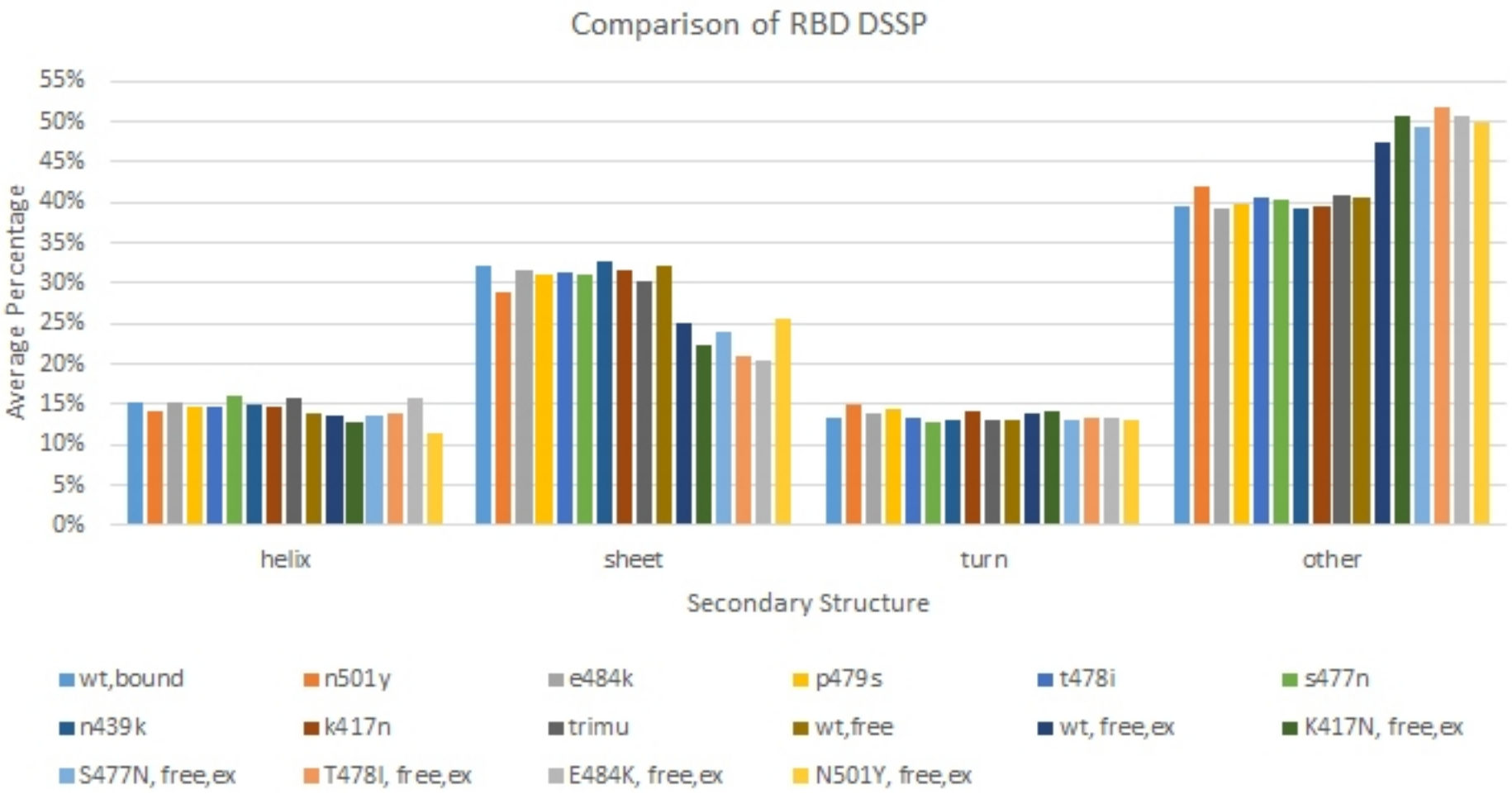
Comparison of RBD DSSP
55%
50%
45%
40%
35%
30%
25%
20%
15%
10%
5%
0%
Average Percentage
helix
sheet
turn
other
Secondary Structure
wt,bound
n501y
e484k
p479s
t478i
s477n
n439k
k417n
trimu
wt,free
wt, free,ex
K417N, free,ex
S477N, free,ex
T478I, free,ex
E484K, free,ex
N501Y, free,ex

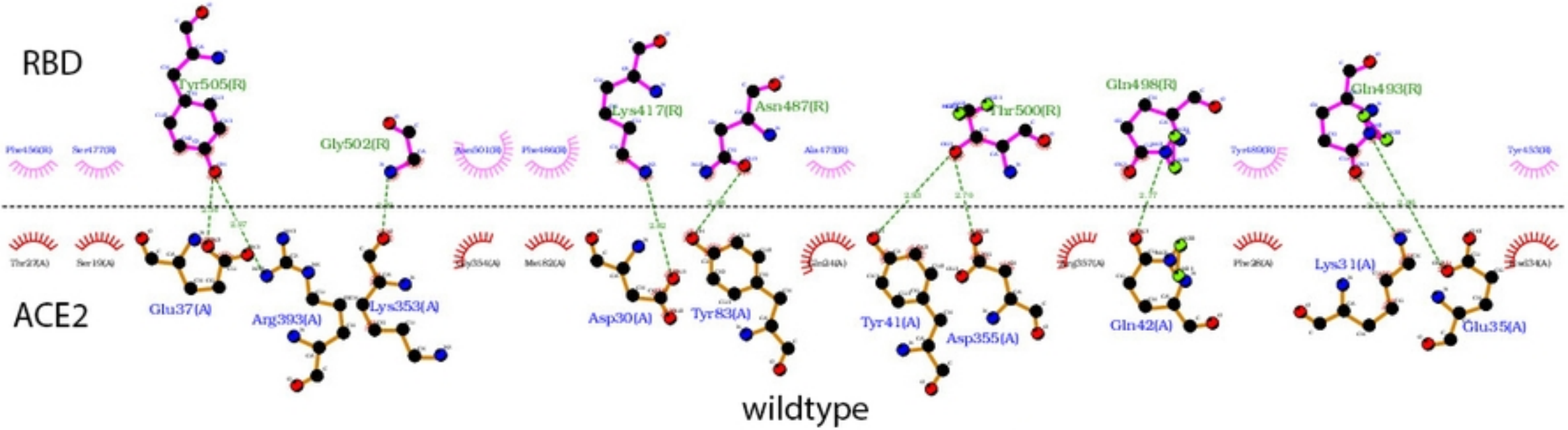

wildtype

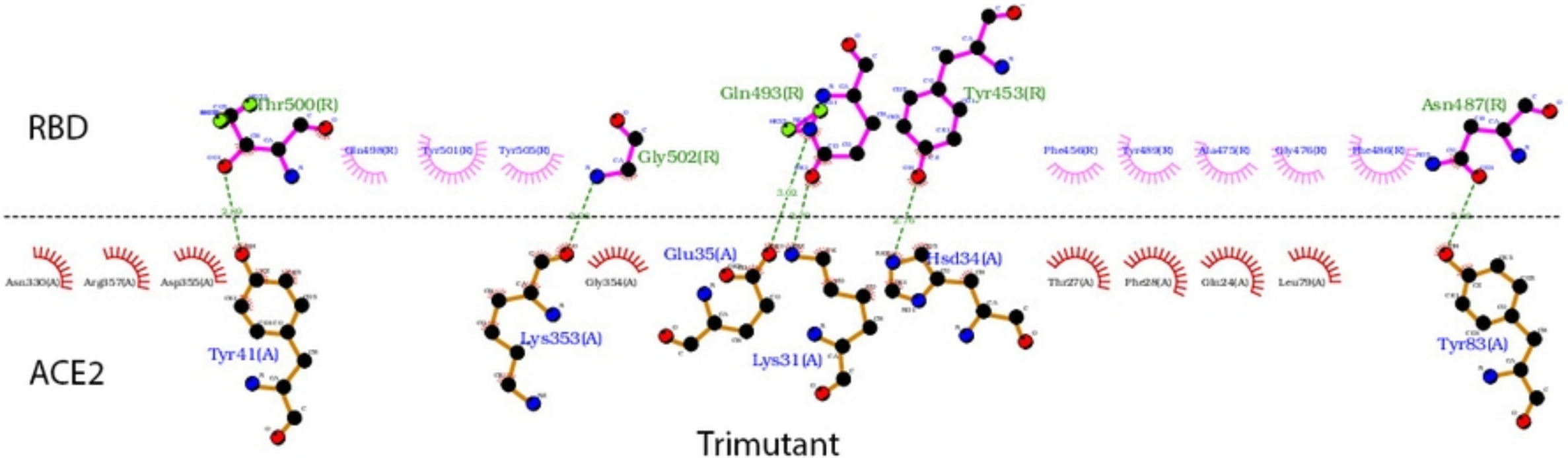

Trimutant

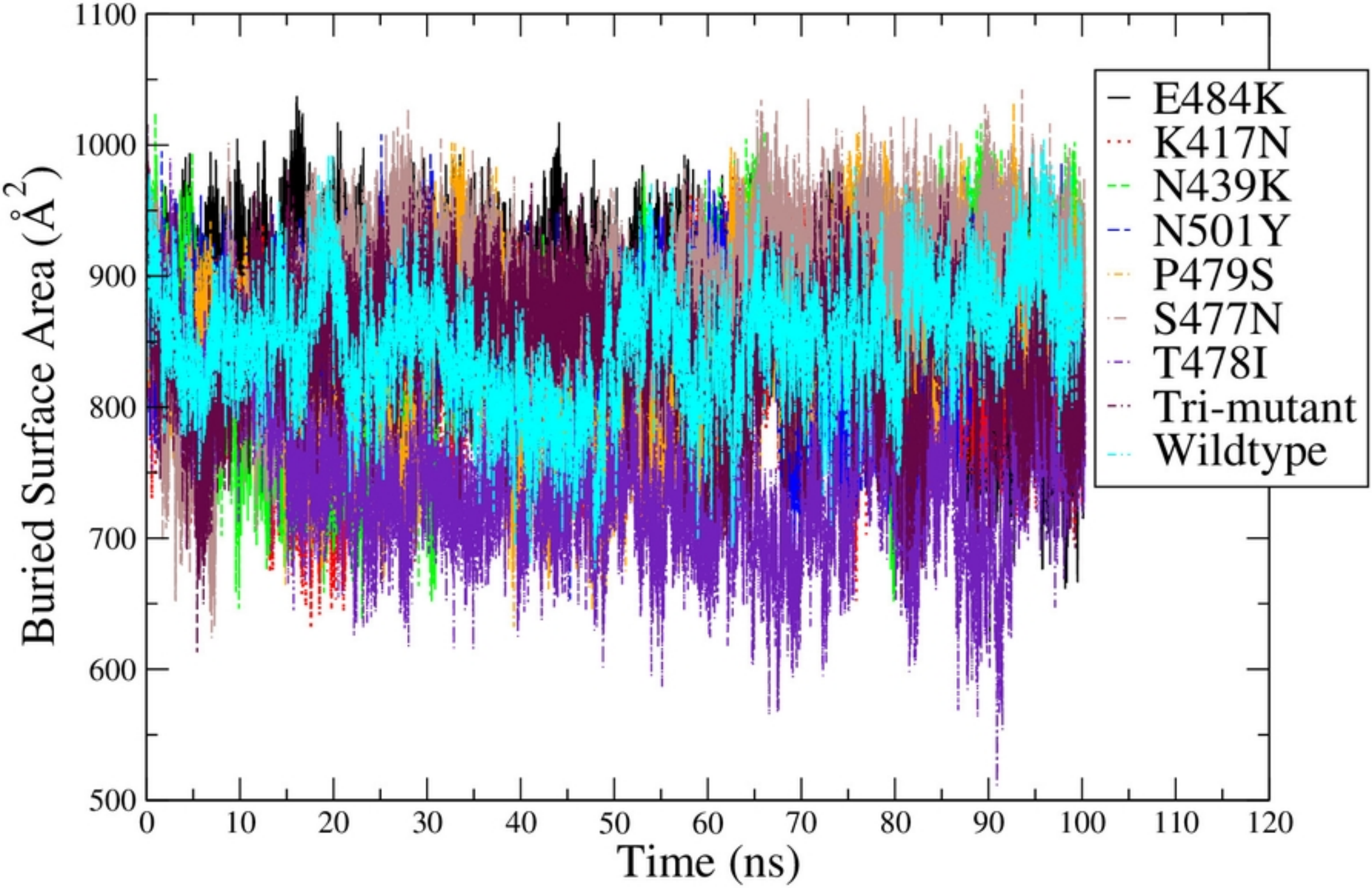
Buried Surface Area (Å^2)
Time (ns)
1100
1000
900
800
700
600
500
0
10
20
30
40
50
60
70
80
90
100
110
120
E484K
K417N
N439K
N501Y
P479S
S477N
T478I
Tri-mutant
Wildtype

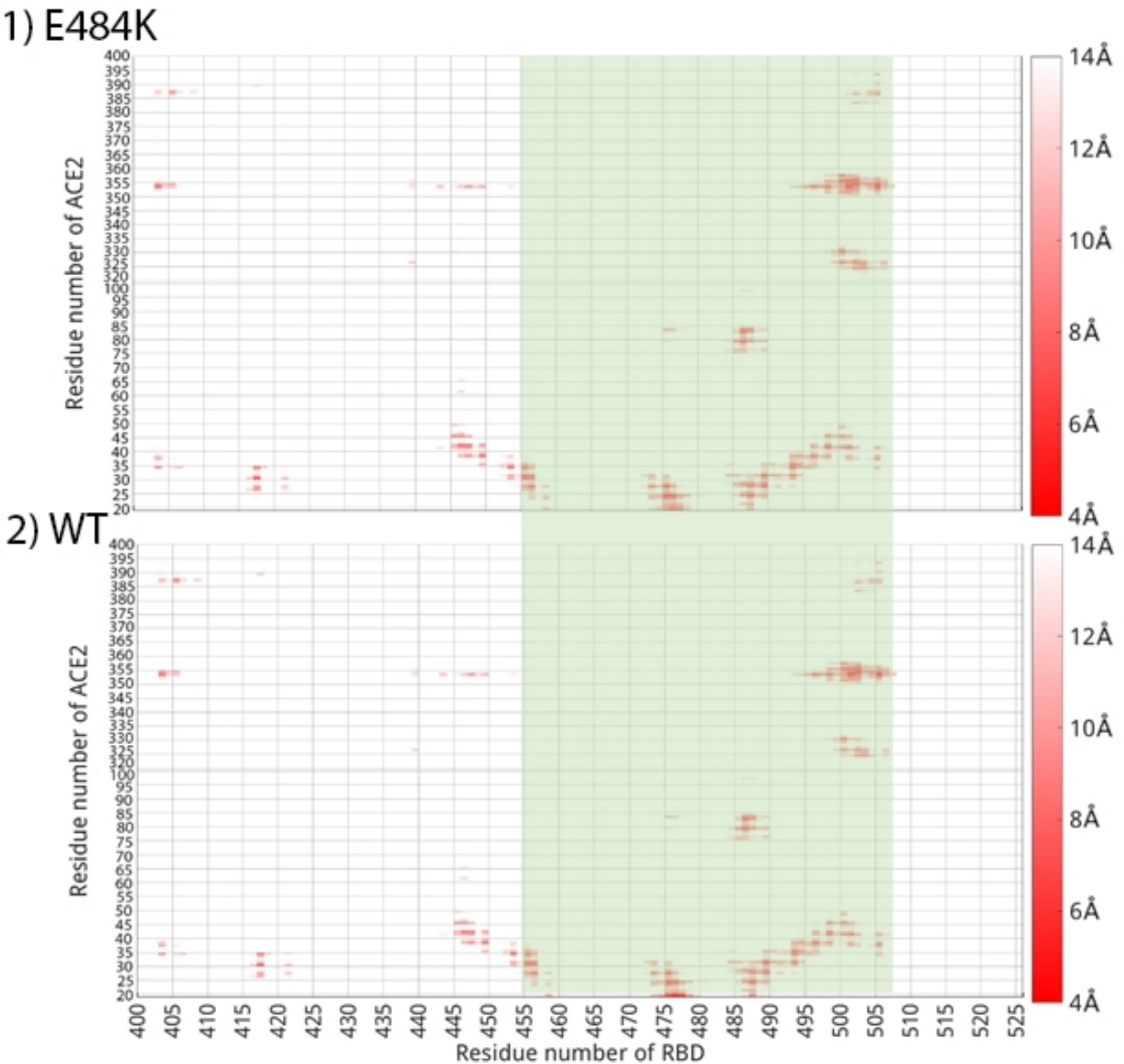
1) E484K
2) WT
Residue number of ACE2
Residue number of RBD
14Å
12Å
10Å
8Å
6Å
4Å

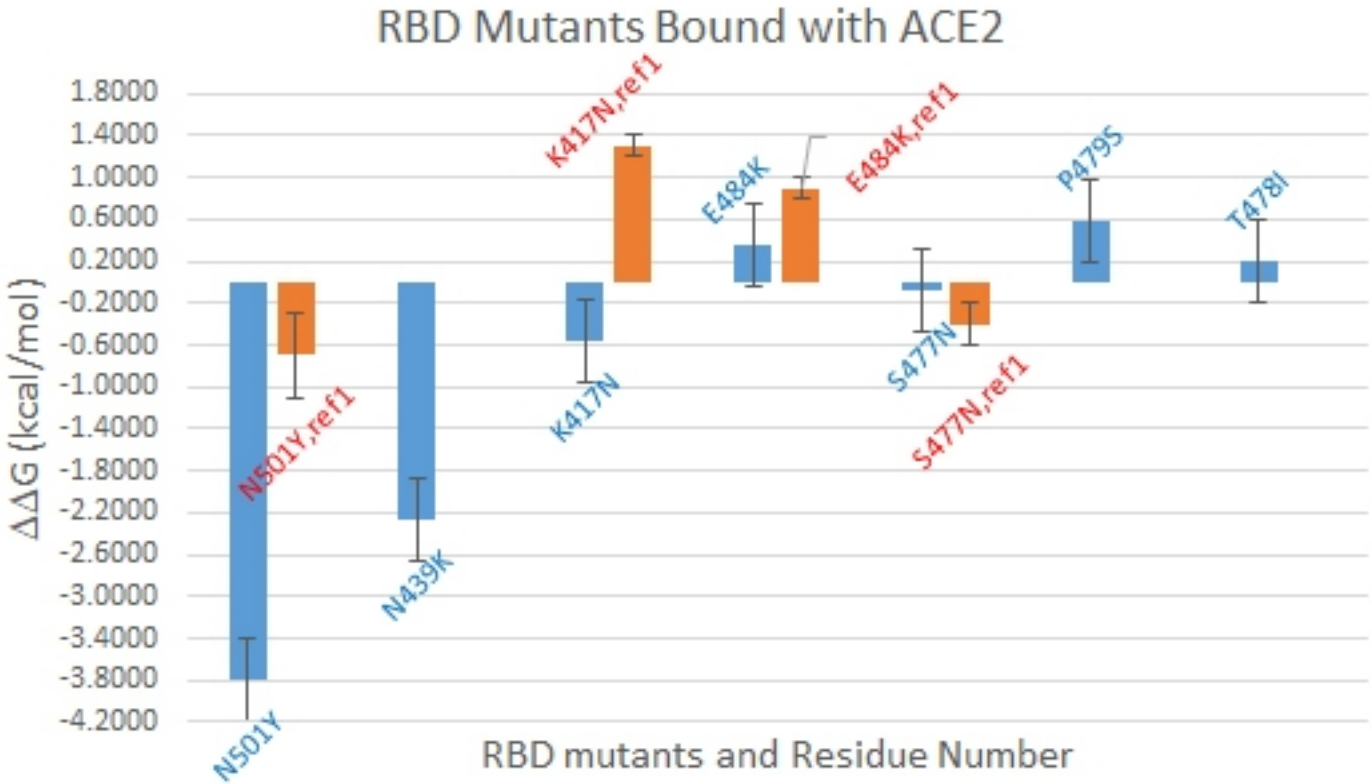
RBD Mutants Bound with ACE2
ΔΔG (kcal/mol)
1.8000
1.4000
1.0000
0.6000
0.2000
-0.2000
-0.6000
-1.0000
-1.4000
-1.8000
-2.2000
-2.6000
-3.0000
-3.4000
-3.8000
-4.2000
N501Y
N501Y,ref1
N439K
K417N
K417N,ref1
E484K
E484K,ref1
S477N
S477N,ref1
P479S
T478I
RBD mutants and Residue Number

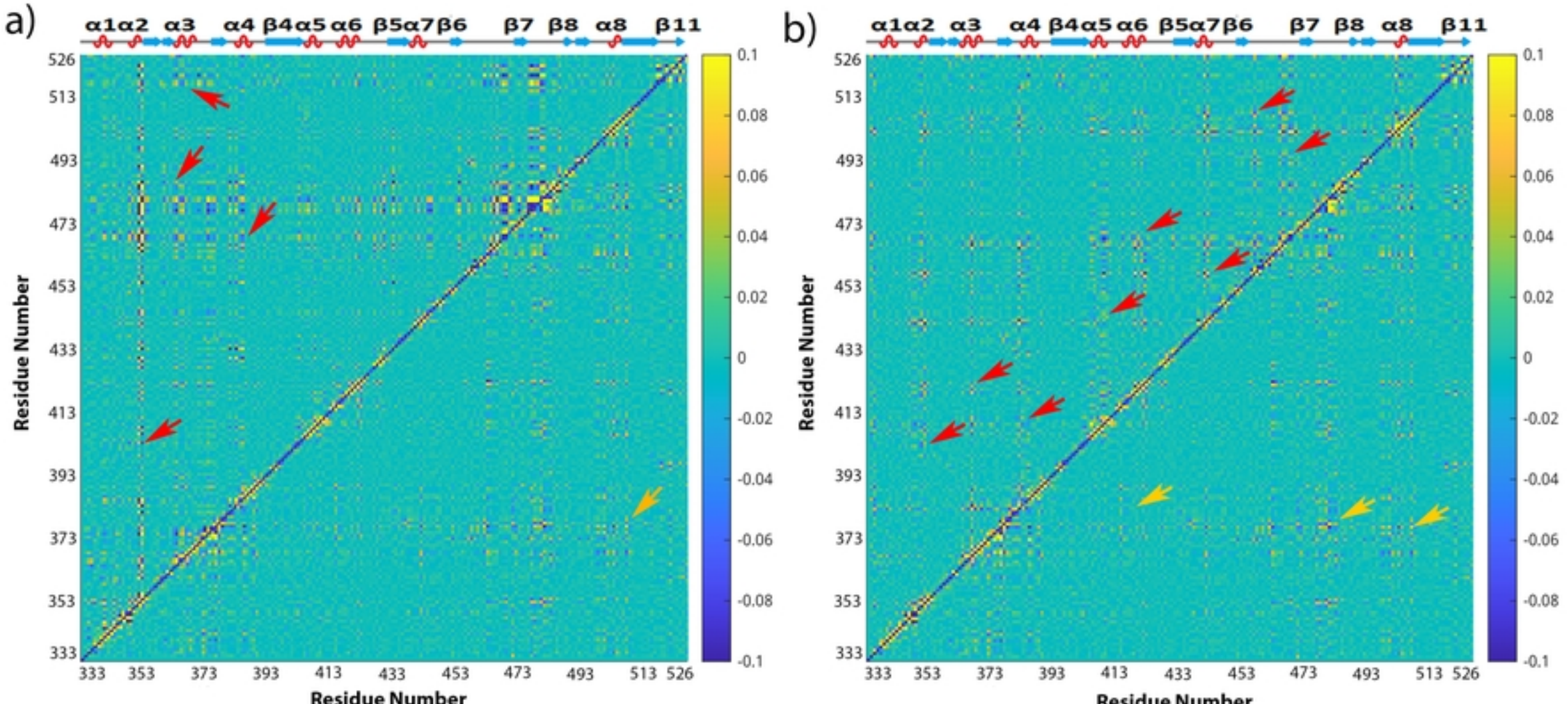
a)
b)
α1α2 α3 α4 β4α5 α6 β5α7β6 β7 β8 α8 β11
Residue Number
333 353 373 393 413 433 453 473 493 513 526
0.1 0.08 0.06 0.04 0.02 0 -0.02 -0.04 -0.06 -0.08 -0.1

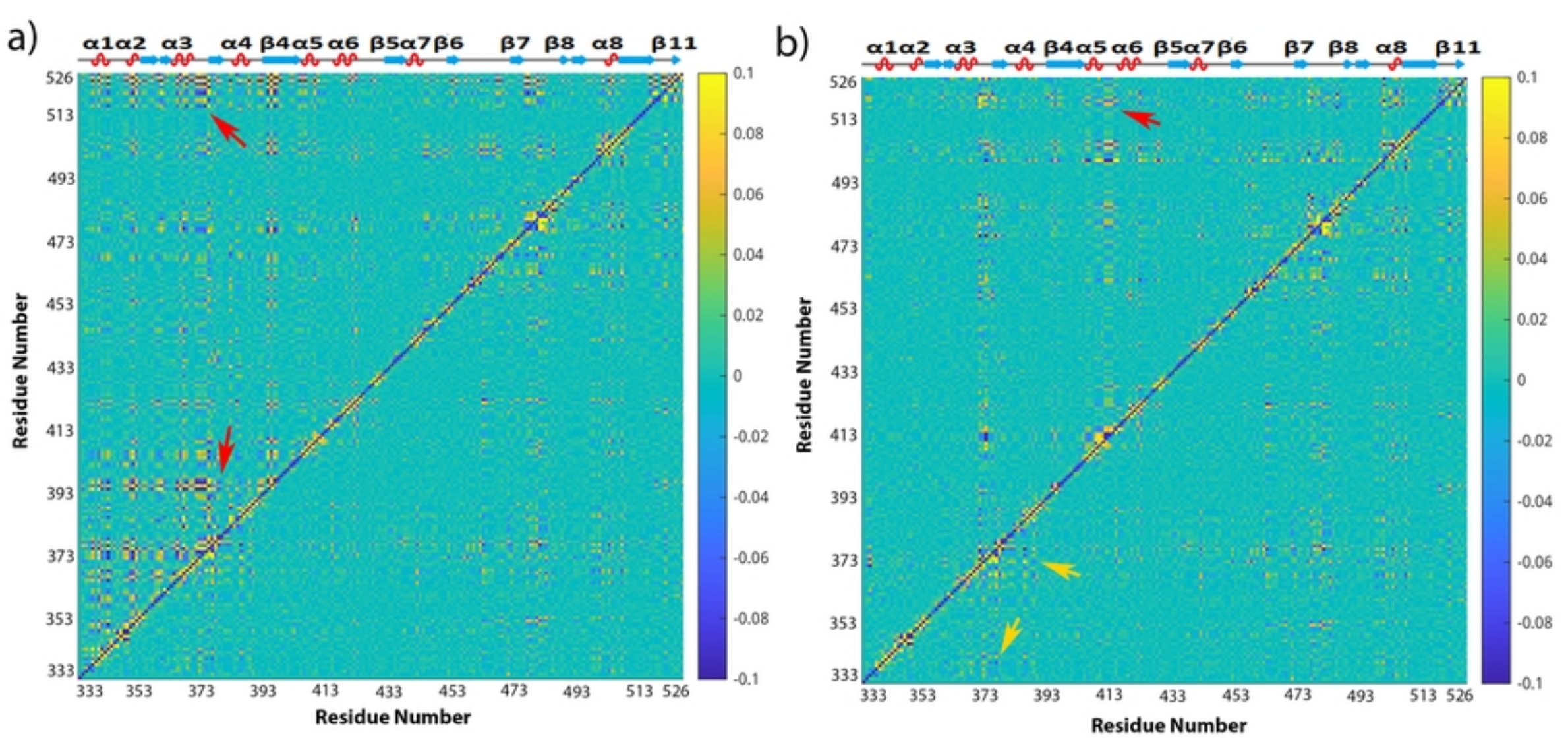
a)
α1α2 α3 α4 β4α5 α6 β5α7β6 β7 β8 α8 β11
Residue Number
Residue Number
526
513
493
473
453
433
413
393
373
353
333
333 353 373 393 413 433 453 473 493 513 526
0.1
0.08
0.06
0.04
0.02
0
-0.02
-0.04
-0.06
-0.08
-0.1
b)
α1α2 α3 α4 β4α5 α6 β5α7β6 β7 β8 α8 β11
Residue Number
Residue Number
526
513
493
473
453
433
413
393
373
353
333
333 353 373 393 413 433 453 473 493 513 526
0.1
0.08
0.06
0.04
0.02
0
-0.02
-0.04
-0.06
-0.08
-0.1

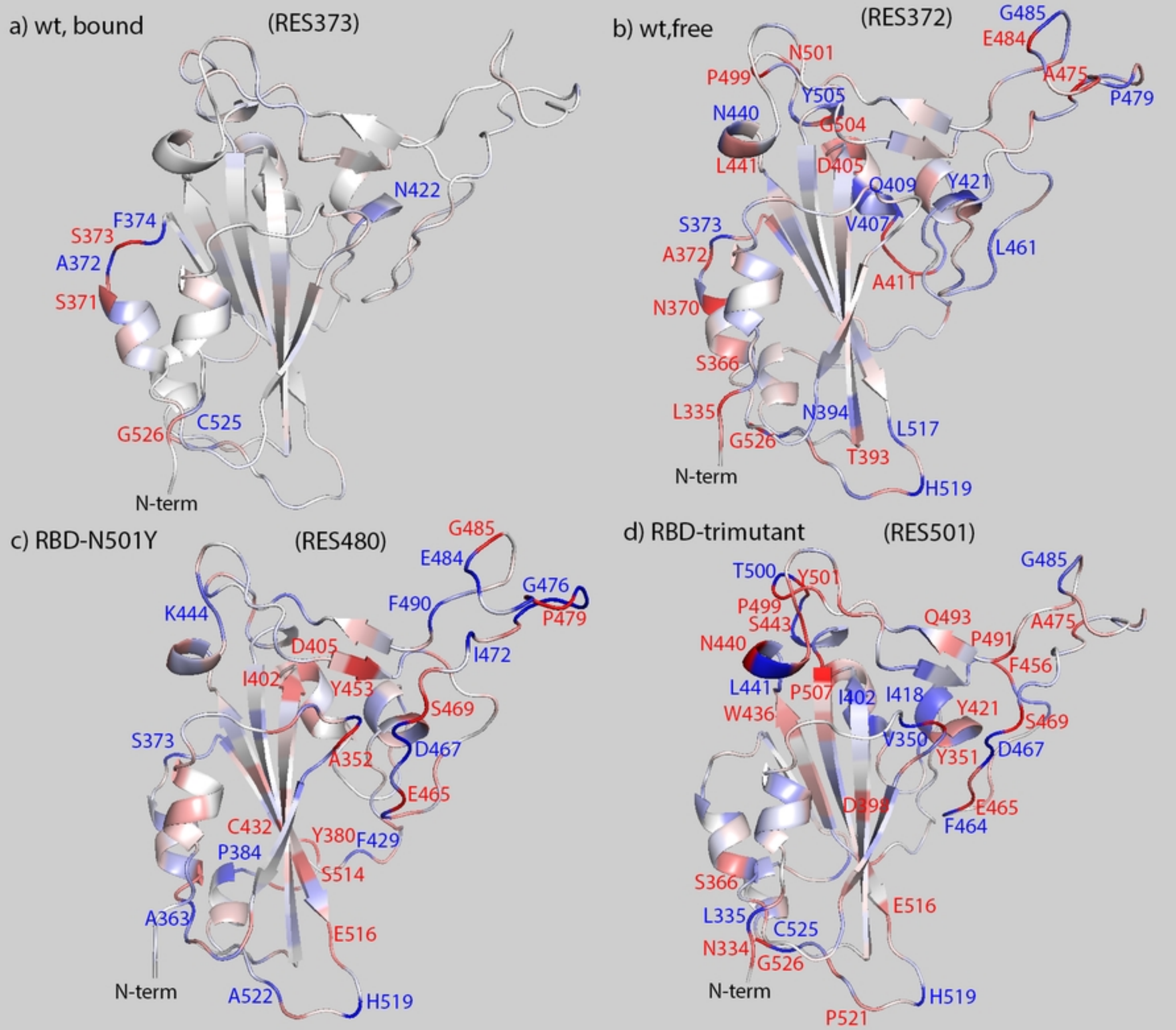
a) wt, bound
(RES373)
F374
S373
A372
S371
N422
C525
G526
N-term
b) wt,free
(RES372)
G485
E484
N501
P499
A475
P479
Y505
N440
G504
L441
D405
Q409
Y421
S373
V407
A372
L461
A411
N370
S366
L335
N394
L517
G526
T393
N-term
H519
c) RBD-N501Y
(RES480)
G485
E484
G476
K444
F490
P479
D405
I472
I402
Y453
S469
S373
D467
A352
E465
C432
Y380
F429
P384
S514
A363
E516
N-term
A522
H519
d) RBD-trimutant
(RES501)
T500
Y501
G485
P499
S443
Q493
A475
N440
P491
F456
L441
P507
I402
I418
Y421
W436
S469
V350
Y351
D467
D398
E465
F464
S366
E516
L335
C525
N334
G526
N-term
H519
P521

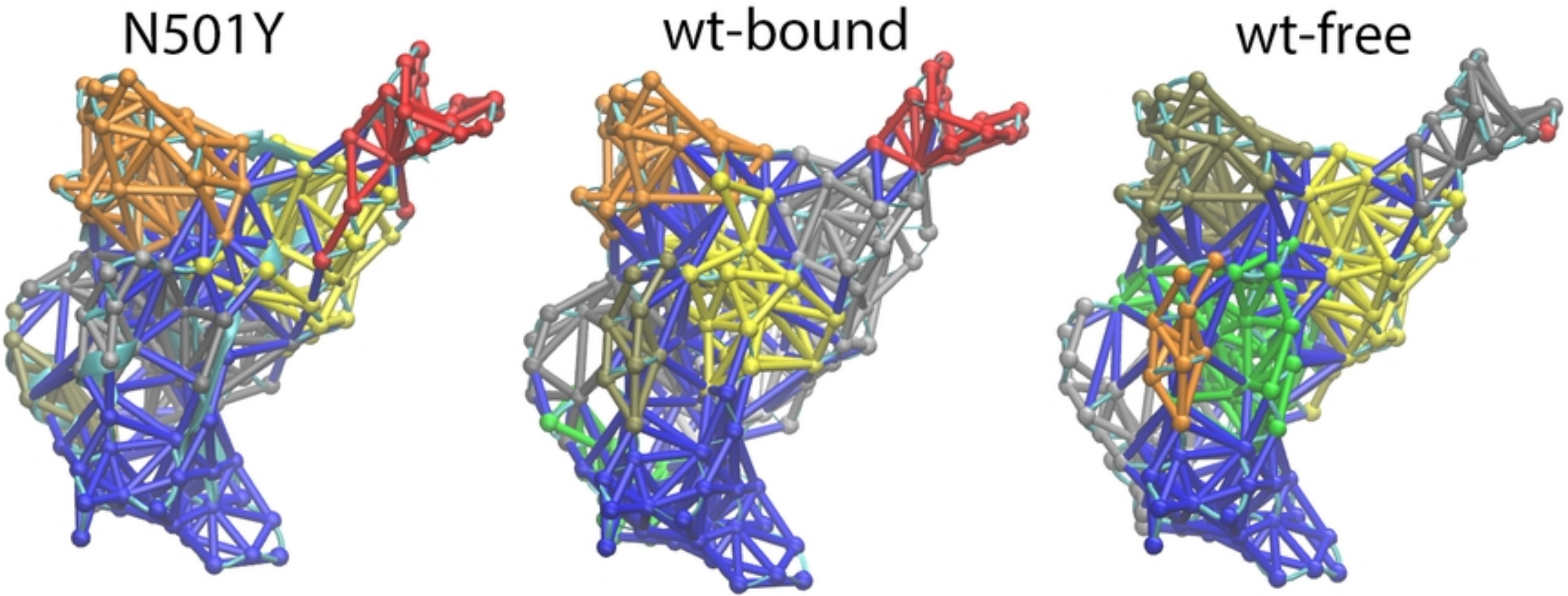
N501Y
wt-bound
wt-free